Basic Res Cardiol (2016) 111:46
DOI 10.1007/s00395-016-0565-2

REVIEW

High field magnetic resonance imaging of rodents in cardiovascular research

Laetitia Vanhoutte[1,2] · Bernhard L. Gerber[3,4] · Bernard Gallez[5] · Chrystelle Po[6] · Julie Magat[7] · Balligand Jean-Luc[2] · Olivier Feron[2] · Stéphane Moniotte[1]

Received: 27 July 2015 / Accepted: 1 June 2016 / Published online: 10 June 2016

Abstract Transgenic and gene knockout rodent models are primordial to study pathophysiological processes in cardiovascular research. Over time, cardiac MRI has become a gold standard for in vivo evaluation of such models. Technical advances have led to the development of magnets with increasingly high field strength, allowing specific investigation of cardiac anatomy, global and regional function, viability, perfusion or vascular parameters. The aim of this report is to provide a review of the various sequences and techniques available to image mice on 7–11.7 T magnets and relevant to the clinical setting in humans. Specific technical aspects due to the rise of the magnetic field are also discussed.

✉ Laetitia Vanhoutte
laetitia.vanhoutte@uclouvain.be

[1] Department of Paediatric Cardiology, Cliniques universitaires Saint Luc, Université Catholique de Louvain (UCL), Brussels, Belgium

[2] Pole of Pharmacology and Therapeutics (FATH), Institute of Experimental and Clinical Research (IREC), Université Catholique de Louvain (UCL), Brussels, Belgium

[3] Division of Cardiology, Cliniques universitaires Saint Luc, Université Catholique de Louvain (UCL), Brussels, Belgium

[4] Pole of Cardiovascular Research (CARD), Institute of Experimental and Clinical Research (IREC), Université Catholique de Louvain (UCL), Brussels, Belgium

[5] Biomedical Magnetic Resonance Unit (REMA), Louvain Drug Research Institute (LDRI), Université Catholique de Louvain (UCL), Brussels, Belgium

[6] CNRS, ICube, FMTS, Institut de Physique Biologique, Faculté de Médecine, Université de Strasbourg, Strasbourg, France

[7] L'Institut de RYthmologie et de Modélisation Cardiaque (LIRYC), Inserm U1045, Bordeaux, France

Keywords High field · MRI · Cardiovascular diseases · Mouse

Abbreviations

ASL	Arterial spin labeling
CEST	Chemical exchange saturation transfer
CS	Compressed sensing
CT	Computed tomography
DENSE	Displacement encoding with stimulated echoes
FLASH	Fast low angle shot
FPP	First pass perfusion
IR	Inversion recovery
LGE	Late gadolinium enhancement
MBF	Myocardial blood flow
MEMRI	Manganese-enhance magnetic resonance imaging
MRA	Magnetic resonance angiography
MRS	Magnetic resonance spectroscopy
MRSI	Magnetic resonance spectroscopic imaging
PET	Positron emission tomography
PC	Phase contrast
RF	Radiofrequency
SNR	Signal-to-noise ratio
SPIONs	Superparamagnetic iron oxide nanoparticles
TOF	Time of flight
HF	High field
Venc	Velocity encoding

Introduction

Transgenic and knockout mice models are currently fundamental tools to study pathophysiological processes and therapeutic interventions in cardiovascular research. In recent years, high field (HF) MRI has evolved to become

an essential tool for experimental imaging, with an increase in reported studies characterizing these small animal models with MR systems operating at 7 T or higher. Indeed, since its introduction in the 1970s by Paul C. Lauterbur and Sir Peter Mansfield, improvements have led to spectacular development of MRI technology, allowing now to image hearts of rodents (<200 mg weight) in vivo at heart rates up to 600 bpm. The specific advantages of HF cardiac MR over other techniques such as echocardiography are its high accuracy and reproducibility [7, 137] and large versatility with the ability to provide insight into many physiological processes. Similar to human low-field CMR, HF CMR in rodents allows comprehensive evaluation of various parameters by different pulse sequences, not only allowing assessment of systolic and diastolic function but also of myocardial perfusion, viability, flow and molecular imaging [4, 44, 98, 116, 148, 159]. This work is primarily addressed to nonspecialist readers who have basic knowledge in (clinical) MRI and cardiology and are likely to perform cardiac HF MRI on small experimental animals. Basic principles of MRI [151] and thorough technical aspects [14] have been reviewed elsewhere. Here, we seek to provide a general overview of current imaging techniques and sequences available for HF imaging in mice and to define their interest in connection with clinical applications in humans.

Technical considerations

Hardware

HF MR Systems are dedicated small bore magnets allowing animal imaging at very high field strengths (>7 T). The main advantage of increasing field strength for MR imaging is the increased signal-to-noise ratio (SNR) allowing higher resolution. The downtrades are greater field inhomogeneity and susceptibility to artifacts and higher radiofrequency (RF) power deposition in tissue—measured by the specific absorption rate (SAR) [101]. Overall, although some authors report nice image acquisitions at clinical field strength (1.5–3 T) with optimized coils [29, 53, 62], or at the very high field of 17.6 T [60, 61], it is generally admitted that the range of 7–11.7 T offers the best trade off for most applications in small animals [48]. Systems can be either horizontally or vertically mounted. Vertical position of the magnet (as encountered in some biochemistry-based core facilities) although unphysiological and less practical for monitoring and customizing the probes, does not seem to interfere with cardiac hemodynamics [123, 173].

Various RF coil designs have been proposed to maximize SNR: surface coils, linear volume coils or birdcages [46, 98]. CMR in mice using a cryogenic quadrature RF coil has also been reported, offering significant gain in SNR compared to conventional coils operating at room temperature (see "Improving imaging speed: parallel imaging, compressed sensing (CS) and cryoprobes") [167]. In small animals applications, mid-range coils are usually used, which means that the product (fd) of the frequency f and the coil diameter d is in the range 2–30 MHz-m.

Animal handling and gating strategies

Small animal CMR is particularly demanding in terms of experimental setup installation and recording of vital parameters, in particular because of the small body size of the animals and their high cardiac and respiratory frequency, which increases the magnitude of motion artifacts.

To perform CMR procedures in living animals, general anesthesia is required throughout the acquisition. Currently, the preferred approach is isoflurane inhalation, because it causes minimal hemodynamic depression, allows short induction and fast awakening times, together with and easy regulation of anesthesia depth [74, 85]. In general, anesthesia is induced by placing the animal in a closed container using 3–5 % isoflurane for 2–3 min. Then the animal is installed in the scanner and anesthesia is maintained by continuous inhalation of 0.5–1.5 % isoflurane through a nose cone. Because anesthesia leads to rapid heat loss, the core body temperature must be carefully followed with a rectal probe and regulated by external heating with a heating blanket. ECG signal and other vital parameters can be recorded with specific monitoring systems. ECG electrodes are wrapped around the paws. During anesthesia, the rodents remain under spontaneous breathing, and respiratory rate is monitored by pneumatic sensor placed under the animal. The depth of anesthesia is modulated during the examination to remain within physiological heart rates (around 400–600 heartbeats/min) and respiration rates (around 50–100 cycles/min). This is allowed to remain within the physiological loading and pressure states, and ensures a proper reproducibility of the data [34, 163]. ECG and respiration gating signals can be integrated in the MR systems to allow prospective or retrospective trigger of the MRI acquisition, and minimize motion artifacts as breath holding is impossible in small animals.

Because at HF ECG signal is often degraded by the magnetohydrodynamic effects, RF pulses, and gradient switching during scanning [53], alternative techniques to the classical gating have been reported for rodents, using optimized gating strategies with cardiorespiratory monitoring [6, 33] or complete monitoring-free approaches [63–65, 103]. Optimized approaches developed to speed up image acquisitions are developed in "Improving imaging

speed: parallel imaging, compressed sensing (CS) and cryoprobes".

Evaluation of cardiac volumes, mass and function

The assessment of left ventricular function and volumes is fundamental in the comprehensive evaluation of animal models mimicking human diseases. Because of its high availability and ease, 2D-echocardiography remains the most commonly used noninvasive method for in vivo evaluation of rodent ventricular function. Yet it suffers from well-documented limitations, such as restricted acoustic windows, the need for an experienced operator and geometrical assumptions used to extrapolate data, as generally only 2- and 4-chambers long-axis slices or parasternal M-mode images can be acquired. CMR, being a true three-dimensional imaging technique, with an unrestricted access to the heart from all directions allows acquisitions in various directions (i.e., 4-, 3-, 2-chambers long axis and continuous stacks of serial short-axis images), and therefore, provides a better reproducibility [7, 137, 150] of measurements of the biventricular volumes and masses.

CMR assessment of biventricular function is typically acquired using segmented k-space fast gradient echo sequence (fast low angle shot—FLASH) with short TE, either with prospective gating or self-gated navigator sequences with retrospective reordering of images, applied to obtain short-axis views covering the entire left and right ventricular volumes. Temporal resolution of 10–20 phases per heartbeat (i.e., 5–10 ms) can be obtained, while spatial resolution typically approximates 0.1–0.2 mm. Generally, a stack of 6–8 serial 1 mm-thick short-axis slices is prescribed to cover the entire left and right ventricles. Ventricular volumes and masses are usually derived using Simpson's method where endocardial and epicardial borders are drawn on serial short-axis slices and volumes are derived by summing compartment area multiplied by slice thickness (Fig. 1). Masses can be extrapolated as the myocardial volume (difference between epicardial and endocardial volumes) multiplied by the myocardial specific density (1.05 g/cm^3).

Serial assessments of systolic function in various mouse models have already been described in the literature, even in neonatal mice [175], and have proved high accuracy in comparison to phantom measurements [120], ex vivo data [120, 123, 163] and invasive flow measurements [104]. The

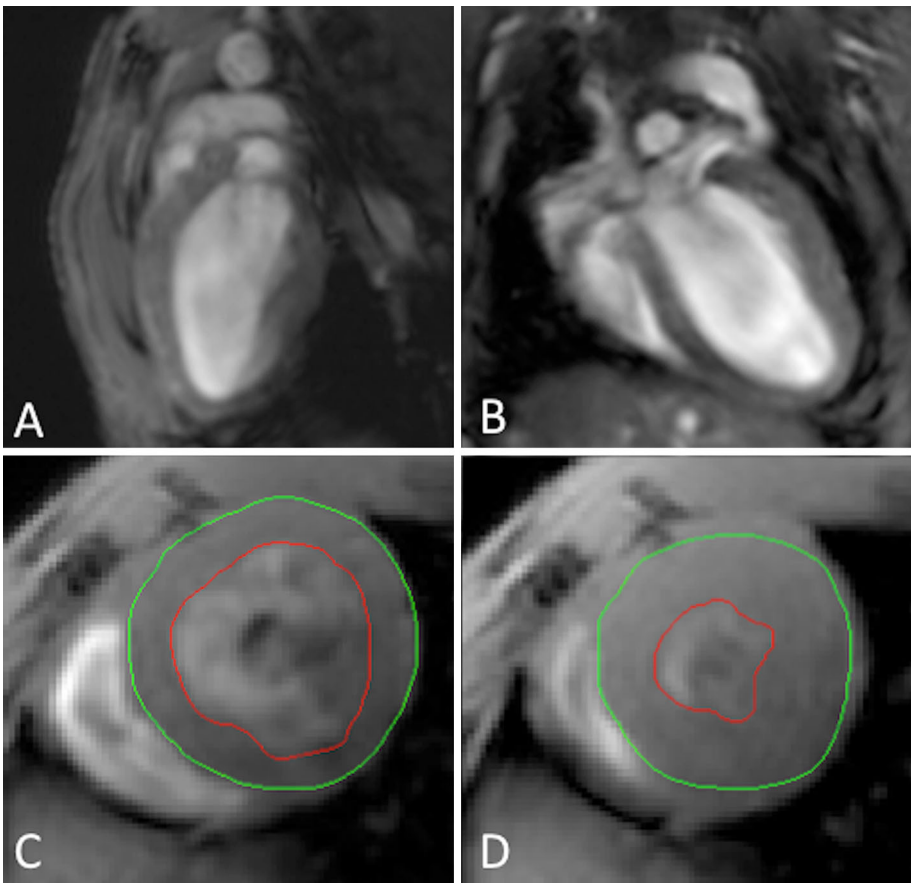

Fig. 1 Long axis two-chamber (**a**), long axis four-chamber (**b**) and short-axis (**c**, **d**) views of mouse hearts obtained with a FLASH sequence, at 11.7 T (Biospec, Bruker, Ettlingen, Germany). Endocardial (*red*) and epicardial (*green*) outlines were drawn in end-diastolic (**c**) and end-systolic (**d**) phases. Imaging parameters: TE/TR 1.5 ms/4.1 ms; FOV 30.0 × 30.0 mm; slice thickness 1.25 mm

high reproducibility of the method has also been assessed in several publications [59, 120, 123, 150, 163]. Therefore, the technique is ideally applied to study genetic, pharmacological or surgical interventions in mouse models of cardiovascular diseases.

By contrast, diastolic function assessment by CMR in rodents remains challenging. Drelicharz and colleagues reported filling rates (FR) derived from time-area curves obtained in the mid ventricular short-axis plane, as slope of the beginning part of diastolic limbs. They demonstrated that this approach allowed a reliable assessment of diastolic function in a mouse model of dilated cardiomyopathy at 4.7 T [47, 147] and the technique was further successfully used by other teams at higher field [1, 17, 174]. More recently, Buonincontri et al. used a similar (simplified) approach derived from echocardiographic color kinesis (Echo-CK), to measure diastolic index in a mouse model of diabetes ([30], at 4.7 T), a concept previously described and validated in humans [113]. Ideally, these measurements require acquisitions with high temporal resolution ($\geq$20 phases), to improve their reliability. If their use remains limited so far, they could still be easily transposed to other experimental models in the near future.

Intramyocardial function and strain

In models of cardiovascular diseases characterized by inhomogeneous dyskinetic regions in the myocardium, detailed quantification of the regional contractile performance of the heart may bring additional information to functional and volumetric indices. Several approaches are currently available for this purpose.

Tagging

Tagging is a technique in which selective spatial presaturation pulse are noninvasively applied on the image using delays alternating with nutations for tailored excitation (DANTE) [102] or spatial modulation of magnetization (SPAMM) [11] prepulse techniques prior to the acquisition of cine FLASH sequences. This results in stamping the myocardium with orthogonal lines or grid patterns (tags) which can then be followed during the cardiac cycle. Strain and torsion can be quantified with specific methods, such as the harmonic phase (HARP) based analysis [114] (Fig. 2).

The use of this sequence in small rodents at high field remains challenging because of the high heart rate requiring very short echo times to achieve sufficient temporal resolution during the cardiac cycle. Also, these images must be acquired using prospective gating with quality ECG to adequately deposit the tagging pattern in early systole and avoid subsequent taggrid deformation [90]. Furthermore, as a consequence of the small anatomy, very high spatial resolution and small tag spacing are required to characterize the strain. Finally, the post-processing and image analysis need to be adapted to lower SNR.

Some authors described successful applications of tagging sequences to rodents at field strengths $\geq$7 T [90, 132], showing that it can provide more sensitive measures of functional alterations than global functional indexes, helping to better understand the pathophysiology of various cardiovascular diseases, such as dilated cardiomyopathy [37, 57, 58, 141], restrictive cardiomyopathy [69] or cardiac dysfunction accompanying neurodegenerative diseases ([89], at 4.7 T).

Besides conventional tagging, other approaches have also successfully been used for deformation imaging at HF,

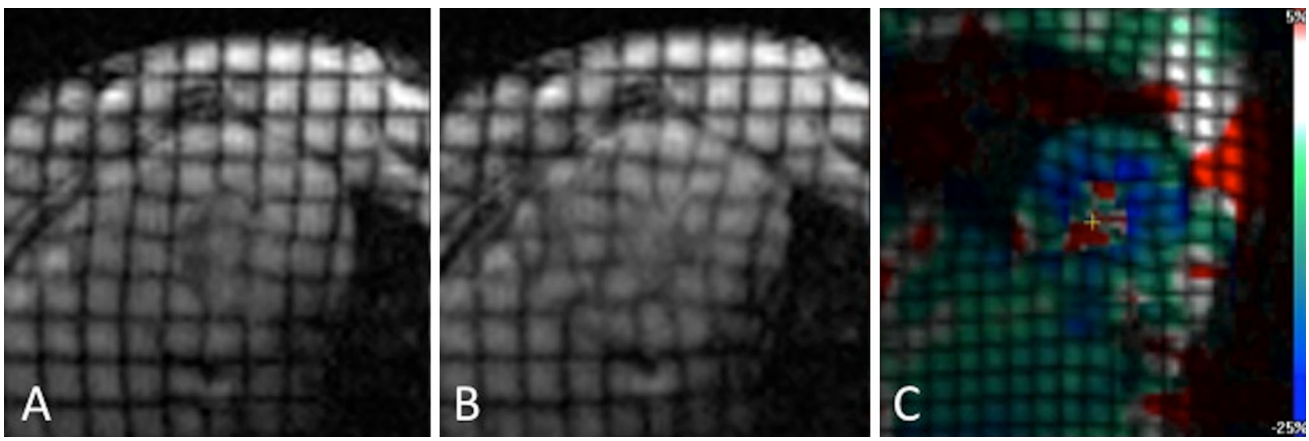

Fig. 2 SPAMM tagged images in mice. Compared to the reference image in end-diastole (**a**), the tag lines show clear contraction and twist of myocardium in end-systole (**b**). Imaging parameters: TE/TR 1.8 ms/12 ms; tag distance 0.3 mm, tag thickness 1 mm. **c** Representative short-axis strain map obtained with HARP software (Diagnosoft, Inc., Baltimore, MD, USA). *Blue zones* correspond to the highest deformation

tissue phase mapping (TPM) and displacement encoding with stimulated echoes (DENSE). Vector-based feature tracking software for strain measurement on classical cine images has also been shown feasible [75, 119].

To our best knowledge, only one study has compared echocardiographic and HF MRI strain measurements in mice. In their work, Azam et al. demonstrated that although echocardiographic vector velocity imaging seemed to be feasible and accurate, strains measured with DENSE method were more variable than those measured with MRI with similar variability for radial and circumferential strains [12].

Displacement encoding with stimulated echoes (DENSE)

DENSE is based on a stimulated echo sequence, in which the displacement of the myocardium is directly encoded into the phase of the MR signal, allowing strain quantification with high spatial resolution [5]. If its preclinical application has been more limited than tagging so far, technical adjustments allowing multiphase application [177], 3D acquisitions [178] and simplified post-processing [52, 140], could allow wider use of DENSE MRI in mice in the future.

Tissue phase mapping (TPM)

Dubbed phase contrast imaging or tissue phase mapping (TPM) provides pixel-wise encoding of the velocity—rather than displacement—in its phase images (see "Phase contrast angiography"). Different studies have successfully determined myocardial velocities in mice at different time point of cardiac cycles using this technique. If first studies were using bright blood contrast [60, 105, 134], blood suppression has been shown to improve accuracy of measurements in further developments [43, 79]. Baseline values of normal transmural wall motion pattern have been carefully established with TPM, allowing further comparison with genetically and surgically manipulated mouse models [43].

Perfusion, stress imaging and tissue characterization

Evaluation of myocardial perfusion and stress response is fundamental for the comprehension of pathophysiology of various models of cardiac disease. Tissue characterization (myocardial viability) and infarct visualization allows the comprehensive understanding of models of ischemic heart disease and subsequent myocardial remodeling.

Perfusion

Myocardial perfusion (i.e., myocardial blood flow per gram of tissue expressed as ml/g/min) is a key parameter in the investigation of cardiac diseases, as it allows characterizing the relationship between blood flow (oxygen delivery) and cardiac contraction in cardiac diseases. Currently, there are two different approaches to evaluate myocardial perfusion using HF CMR: (1) gadolinium-enhanced first pass perfusion (FPP) after the bolus injection of exogen contrast agent through a vein, and (2) arterial spin labeling (ASL) which makes use of intrinsic properties of the protons, and does not require contrast injections.

FPP sequences make use of the intravenous injection of gadolinium chelated contrast agents, which present paramagnetic effects. At moderate doses these agents shorten T1 times of the surrounding tissues in direct proportion to their concentration. At high doses the relation may become nonlinear because of additional T2 and T2* susceptibility effects. In the literature, contrast doses between 0.1 and 0.9 mmol/kg have been used in rodents. Because of the fast systemic blood circulation time (4–5 s) [40] added to the general limitations of cardiac imaging in rodents, HF contrast-enhanced FPP CMR requires very fast acquisitions. At the same time, adequate spatial resolution has to be preserved, to visualize the regional myocardial inflow of the gadolinium. These challenges explain the very recent emergence of studies on FPP CMR in the experimental field. They all rely on rapid acquisition of saturation recovery sequences during the passage of a contrast bolus through the heart. Parameters like myocardial blood flow (MBF), myocardial tissue function (TF) and arterial input function (AIF) could be precisely quantified using dual-bolus [9, 154, 155] or dual-contrast [106] strategies either by tracer kinetic modeling or Fermi function deconvolution [76]. FPP MRI has successfully been applied at HF in mouse models of myocardial infarction [9, 40], cardiac hypertrophy [154] and obesity [106], with a good reproducibility of the regional quantitative perfusion estimates [155].

ASL has been described for more than 10 years to investigate myocardial perfusion in small animals. This approach, described by Bauer et al. [21], and further validated by comparison to the well-established microsphere technique in the isolated heart [20] and in the intact animal [170], does not require injection of external contrast agent, but makes use of modification of the magnetic properties of hydrogen protons circulating in the blood entering the imaging slice. As a consequence, image intensity changes occur depending on blood supply to the tissue. Circulating spins are labeled through an RF impulsion, and the myocardial blood flow (MBF) is detected by comparing the resulting tissue T1 relaxation time change between an

acquisition with labeled and unlabeled protons from adjacent slice. Practically, a gradient echo sequence is used to obtain a stack of images at an array of delay times following slice-selective (SS) and non selective (NS) inversions. Then myocardial perfusion can be measured in ml/g/min through the following formula: $P = (1/T1_{ss} - 1/T1_{ns})T1_{ns}/T1_{blood}\lambda$, where λ is the blood/tissue partition coefficient [48]. At HF, the ASL sequence benefits from a better difference between $T1_{ns}$ and $T1_{SS}$, this increases with the magnetic field strength for a given level of perfusion [159]. Over time, the ASL sequence has been properly applied to measure MBF in different mouse models of cardiovascular diseases, after some methodological adjustments to improve the resolution and scan time [2, 32, 55, 80, 135, 144, 162], with a proven reproducibility [32].

Another technique, the blood oxygen dependent imaging (BOLD), has also been considered an alternative perfusion sequence because of its wide use in functional neuroimaging [19]. It makes use of the modification of T2 times of deoxygenated blood. However, many technical considerations have limited its transfer for cardiac imaging [128]. In particular, at high field, many parameters beside deoxyHb/oxyHb may contribute to susceptibility differences [84], and so far, no cardiac study was published in rodents at HF.

Stress-CMR and cardiac reserve

The acquisition of functional data during inotropic stimulation is useful for the detection of ventricular filling abnormalities and to unmask early dysfunction, not detectable in the resting state. In humans, cardiac reserve is also an effective predictor for survival [72]. Stress imaging can be performed in rodents before and after β1-adrenergic stimulation induced by injection of dobutamine at doses ranging from 4 to 16μg/kg/min intravenously or from 20 to 40μg/kg/min intraperitoneally [147].

Inherent challenges to the use of stress-CMR in rodents are the increase in their already high heart rate, complicating ECG-triggered data acquisition, and the need for reproducible measurements. These difficulties have been overcome by optimization of classic functional sequences for higher temporal resolution. Wiesmann et al. were the first to describe the technique at HF in normal and chronically failing mouse hearts [174]. Other studies have then followed on various models of cardiovascular diseases [131, 136, 143], bringing additional interesting data, inter alia the role played by high-capacity creatine kinase system CK/PCr [143] and the neuronal nitric oxide synthase nNOS ([160], at 4.7 T) in inotropic and lusitropic responses to dobutamine but not in the cardiac function at rest.

Late gadolinium enhancement and myocardial viability

In clinical imaging, late gadolinium enhancement (LGE) CMR is a gold standard for the investigation of myocardial viability, because of its superiority for the detection of small myocardial lesions undetectable with nuclear imaging [126]. Viability is also a key prognostic factor in human cardiovascular diseases.

LGE images are acquired late (at least 10 min) after the intravenous or intraperitoneal injection of gadolinium-based contrast agents. The technique is based on the principle that Gd-chelates have an extravascular distribution volume. Infarcted or fibrotic tissues present reduced cellular and increased extravascular volume, with therefore higher contrast concentrations at equilibrium, translating into shorter T1 times. To obtain optimal T1 weighing contrast between normal and abnormal myocardium, an inversion recovery (IR) technique is applied, nulling the signal intensity for normal myocardium (Fig. 3). Optimal inversion time to null viable tissue is previously defined with a look-locker sequence. This approach—well-established in clinical practice—has been successfully described at HF, validated by the great correlation with ex vivo data, and became soon an accepted modality for the study of preclinical models [24, 35, 54, 112, 117].

Nevertheless, applying this technique at HF to rodents remains quite challenging, as their rapid heart rate often results in suboptimal ECG triggering. This may impact the effectiveness of IR sequences, as they rely on a constant time delay between successive IR pre-pulses. Hence, some authors argue that a classical cine FLASH sequence could be used for LGE in place of IR MRI for infarct size assessment, because of its high spatial and temporal resolution. Indeed, unlike at clinical field strength, it seems to provide similar accuracy at high field while being more robust, faster and easier to use [118]. Whatever the type of acquisition used, LGE brings precious information on the pathophysiology of diseases impairing the viability of the myocardium.

Manganese-enhanced MRI (MEMRI)

Similar to gadolinium, manganese (Mn^{2+}) is paramagnetic and decreases T1 in surrounding tissues. In addition, it is actively pumped through the voltage-gated L-type Ca^{2+} channels in cardiomyocytes. Exploiting these specific properties, manganese-enhanced MRI (MEMRI) has been applied at HF in mice for two main applications. First, dynamic MEMRI allows specific measurement of Ca^{2+} channels activity, using T1-imaging at baseline and after infusion of dobutamine. Signal enhancement relates then to calcium influx and inotropic response [8, 23, 68, 168].

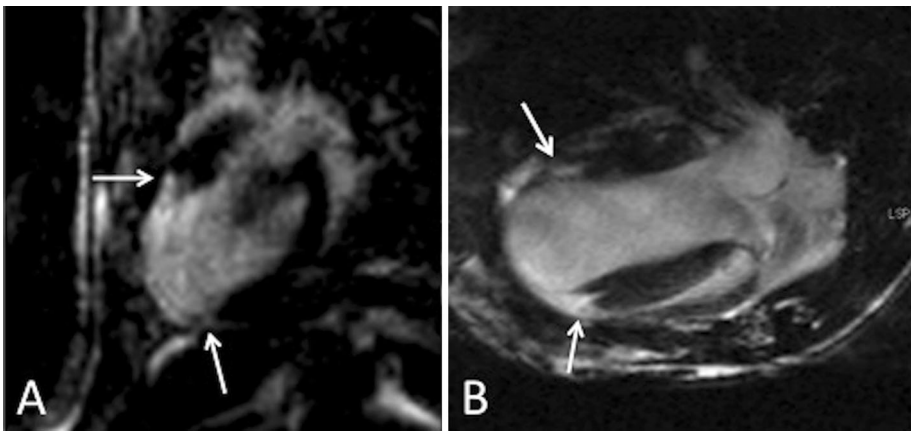

Fig. 3 Long-axis inversion recovery T1-weighted MR image in a mouse with LAD ligation, 20 min after peritoneal injection of a 0.5 mmol/kg bolus of gadolinium DTPA. Limits between the nonviable infarcted myocardium (*hyperenhanced zone*), and the healthy myocardium (*dark zone*) are well visible (*arrows*). Imaging parameters: TE/TR 2.2 ms/4.5 ms, inversion time 350 ms

Second, infarct zone can be accurately delineated after injection of $MnCl_2$, as the uptake of Mn^{2+} is greater in functional regions [67].

Compared to histology, MEMRI is more accurate to determine infarct size than LGE, as the latter tends to overestimate nonviable zone at acute stage. However, unlike MEMRI, LGE has the advantage of showing a decrease in signal when myocardial infarction changes from the acute to the chronic stage [129].

Although MEMRI represents a powerful preclinical tool for the study of ischemic disease, its transfer to the clinical field is hampered by the potential toxicity of free Mn^{2+}.

Relaxometry

The strength of MRI remains its powerful soft tissue contrast, based on the intrinsic relaxation properties T1 and T2. Quantitative measurement of these parameters, also referred to as quantitative relaxometry, can be informative in various pathophysiological processes, and has the advantage of objectively measuring biological changes whereas classical techniques based on qualitative or semiquantitative evaluation may under- or overestimate disease processes. Hence, these last years, T1-, T2- and T2*-weighted imaging already used for clinical applications has emerged in the field of HF CMR in rodents, with or without the use of contrast agents.

T1 mapping

T1 is the longitudinal (or spin–lattice) relaxation time of a tissue. It is known to be prolonged in some conditions like fibrosis, edema and amyloid deposition, and reduced in lipid accumulation, siderosis, hemorrhage and in acute infarction [27]. Parametric maps for T1 are obtained by applying different T1 weighting to a series of images so that each voxel can be assigned a T1 value. They can be displayed using color or threshold scales to enable visual interpretation.

Since the description of the modified look-locker inversion recovery method (MOLLI) by Messroghli et al. [99], which has simplified the acquisition in comparison to the classical look-locker sequence [92], the clinical use of T1 mapping has never stopped to spread. Even if more standardized protocols are needed in this rapidly evolving field, myocardial T1 mapping is already used in numerous hospital centers and has proven its diagnostic and prognostic value in both cardiac diseases (acute coronary syndromes, myocarditis, hypertrophic and dilated cardiomyopathy, congenital heart diseases, heart failure) and cardiac involvement in systemic diseases (amyloidosis, Anderson-Fabry disease, siderosis, diffuse fibrosis of various origins) [49, 100, 121]. In the specific case of diffuse myocardial fibrosis, T1 mapping is considered as superior to the highly invasive and partial endomyocardial biopsies and the indirect technique of LGE. Indeed, it provides a quantitative T1 relaxation time per voxel, instead of a qualitative T1 contrast, allowing discrimination of remaining healthy areas [156].

T1-contrast is also the most used for parametric mapping in mice at HF. T1-mapping is commonly acquired with a sequence based on the look-locker method although some authors described SNAPSHOT-FLASH Inversion Recovery (SNAP-IR) [24, 124] or variable flip angle [39] strategies for the acquisition. In mouse, the acquisition is mainly made in combination with a contrast agent, gadolinium [24, 39, 138] or manganese [8, 77, 87, 88, 168, 169]. Up to now, the technique has been successfully applied to murine models of myocardial infarction [24, 39, 168], cardiac hypertrophy [8, 138] and dystrophinopathy [77]. Various applications have been studied: quantification of infarct size [24, 39, 168], identification of potentially salvageable myocardium [168] and evaluation of monocyte and macrophage spatiotemporal kinetics [107] in the vicinity of a myocardial infarction site,

quantification of focal and diffuse fibrosis [138], or detection of changes in Ca^{2+} channels activity in combination with MEMRI [8, 77, 168, 169]. T1 mapping can also provide valuable information on the pharmacology of contrast agents, and as mentioned earlier, quantitative T1 measurements are essential for perfusion studies based on the ASL technique.

T2 and T2* mapping

Other parametric mappings have not received as much attention as T1-mapping in mice. Nevertheless, they can provide valuable information in the field of cardiovascular research.

T2 is the transversal (or spin–spin) relaxation time. Since T2-weighted imaging is sensitive to liquids, parametric maps for T2 have been described in mouse models of MI to identify edema and area at risk [22, 25, 41, 123], with different strategies of acquisition. It has also been successfully applied to a mouse model of diabetes, with an adequate quantification of fibrosis [28].

Of note, Aguor et al. have also developed a T2* mapping in a mouse model of myocardial infarction, using a multi gradient echo sequence. They showed that T2*-weighted images could be used to discriminate between acute and chronic phase of MI, as a reduction of T2* was observed with infarct age, probably because of the presence of iron [3]. Potential interest of such sequence in mouse models of chronic iron overload has also been assessed at field <7 T [110], but still need further validation at HF, as T2* is very sensitive to large scale magnetic field homogeneities, and may be difficult to measure in case of high iron concentration, as signal decay may become rapid [130].

MR angiography

The increasing number of transgenic murine models mimicking vascular pathophysiological processes, and the growing awareness of the importance of some hemodynamic parameters as independent prognostic factors for morbidity and mortality in cardiovascular diseases [164] has led to an interest in developing reliable MRI techniques for the study of vascular parameters in rodents. If gadolinium-enhanced angiography is often used in the clinical field, the very fast washout of conventional low-molecular weight contrast agents such as Gd-DTPA after injection renders it difficult to apply to rodents [66]. Together with the high cost of contrast agents, these limitations have led to a wider use of non-contrast MR angiography (MRA) sequences in preclinical studies, i.e., time of flight (TOF) and phase contrast (PC) angiography.

Time of flight angiography

The TOF angiography technique is based on inherent vessel contrast resulting from the inflow effect. A flow-compensated gradient echo sequence is applied to a volume with a very short repetition time, saturating the stationary tissue, whereas longitudinal magnetization remains maximal in moving spins. Images obtained are combined using a technique of reconstruction such as maximum intensity projection (MIP) resulting in a 3D angiogram.

Classical limitations of TOF angiography are the signal loss due to spin dephasing when flows are turbulent or too slow and the progressive saturation of the blood signal in the imaging volume leading to a loss of contrast in the distal regions. However, at HF, the angiogram quality clearly benefits from the higher SNR and longer T1 relaxation times of background tissues [166]. In addition, preparation techniques have been developed to enhance the vessel-to-background contrast and its uniformity [122, 145].

If in preclinical studies TOF-MRA is widely used for the characterization of cerebral vasculature, it has also been applied with success to various murine models of cardiovascular disease, including mice with carotid artery ligation [71, 145, 149], hindlimb ischemia [71], aortic aneurysms [82, 83] and/or mice with a hyperlipidemic pattern [149]. A TOF 3D angiogram of the aortic root obtained in a mouse model of aortic banding on an 11.7 T MRI machine is shown in Fig. 4. In such models, the sequence allows longitudinal study of regional neovascularization processes and vessel stenosis or dilation. Moreover, Lefrançois et al. were able to generate a murine whole-body angiogram [86], while Cochet et al. have characterized mice coronary arteries with a high spatial resolution (80μm) TOF-MRA. They further assessed left coronary artery velocity measurements and coronary flow velocity reserve through dynamic MR angiography at seven successive phases throughout the cardiac cycle [38]. The same method of in vivo quantification of blood velocity based on a series of TOF acquisitions was already reported in 2009 by Parzy et al. in mouse carotids and pulmonary arteries [115], bringing evidence that the TOF technique can be more than an anatomical sequence.

Phase contrast angiography

PC-MRA is a functional sequence allowing flow and velocity measurements. This is performed by applying a bipolar gradient that causes moving spins to receive magnetization dephasing, proportional to their velocity. The principle may be applied in all three directions (in- and through-plane) and requires the repetition of sequences with and without flow encoding to generate, respectively, magnitude (anatomical) and phase (quantitative) images (Fig. 5). The encoding gradients are set by the user to

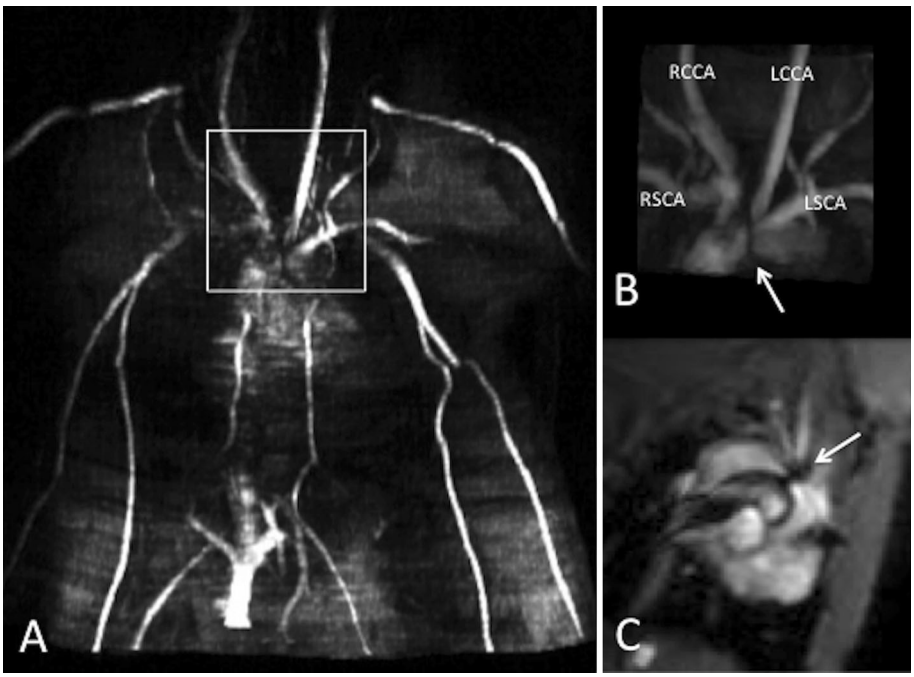

Fig. 4 **a** 3D maximum intensity projection (MIP) of a TOF angiography of the trunk in a mouse (anterior view). *Blurring* corresponds to artifacts due to heart motion. Imaging parameters: TE/TR 2.4/12 ms; matrix 256 × 256 × 120, slice thickness 0.4 mm, flip angle 80°. **b** Details of the aortic arch and the supra-aortic vasculature, showing the transverse aortic stenosis due to surgical banding (*arrow*). *LCCA* left common carotid artery, *RCCA* right common carotid artery, *LSCA* left subclavian artery, *RSCA* right subclavian artery. **c** Sagittal view of the aorta with FLASH sequence, in the same animal. The *arrow* indicates the transverse aortic constriction

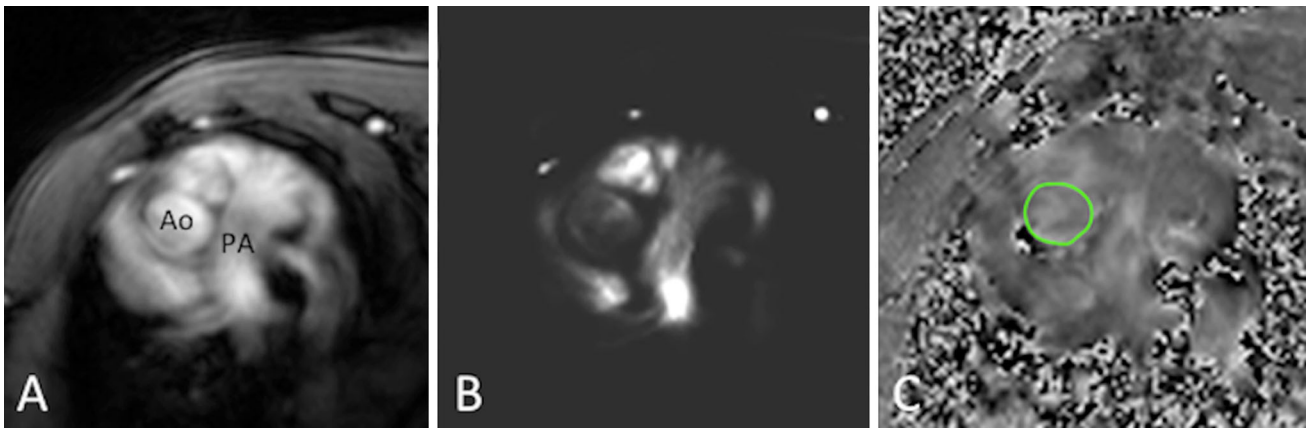

Fig. 5 Transverse FLASH view of the mouse ascending aorta (**a**) and corresponding phase contrast magnitude (**b**) and phase images (**c**). The region of interest where aortic flow measurement can be performed is indicated in *green* on the phase image. *Ao* aorta, *PA* pulmonary artery. Imaging parameters: TE/TR 2.3/8.7 ms, spatial resolution 0.138 mm/pixel, slice thickness 1 mm, VENC 250 cm/s

encode flows within a certain velocity range from −Venc (velocity encoding) to +Venc. These Venc values must be chosen adequately as flow outside this range of values will present velocity aliasing (or wraparound).

Measuring blood flow velocities (BFV) in rodents is challenging, as velocities in the mouse aortic arch are similar to those found in human (about 100 cm/s) [73] while the anatomy is extremely small with aortic cross-sections of a few millimeters square. For years, Doppler ultrasound has been largely used to obtain vascular parameters in small animals' models of vascular diseases [139]. Unlike this approach, which is constrained to measuring velocities along transducer orientation, MRI offers the possibility to study vector component of velocity in any spatial orientation. This makes it more accurate in the determination and follow-up of parameters like BFV, wall shear stress (WSS), pulse wave velocity (PWV) or oscillatory shear index (OSI), even in curved vasculature. These valuables indexes are known to be early markers of dysfunction in mice with atherosclerotic patterns [61, 73, 176].

Cellular and molecular imaging

Although MRI has become one of the preferred imaging modalities used in cardiology, its resolution remains insufficient at a cellular or molecular scale, unless detectable probes or spectroscopic measurements are employed.

Superparamagnetic iron oxide nanoparticles (SPIONs)

Over years, different in vivo MRI detectable probes have been considered for molecular or cellular imaging in small animal studies, as conventional methods (LGE, T2-weighted imaging, T2-mapping) remain not specific for a particular type of tissue process or injury. Among them, superparamagnetic iron oxide nanoparticles (SPIONs) represent a powerful tool for cellular MR imaging. After labeling of stem cells with these small biocompatible crystalline magnetite structures, cell engraftment, differentiation and viability can be noninvasively monitored thanks to the high sensitivity of SPIONs for MRI [26]. If so far, cardiovascular applications in mice at HF remain scarce [36, 96, 111, 133, 165], it represents a promising approach for the study and follow-up of stem cell therapy in the field of cardiology.

Magnetic resonance spectroscopy (MRS) and X-nuclei MRI

Magnetic resonance spectroscopy (MRS) has made possible investigation at a molecular level, allowing comprehensive assessment of metabolic changes in vivo, by producing a collection of peaks at various radiofrequencies—the spectrum—representing a considered nucleus in different chemical environments. The peak position is determined by chemical bonds and the area under the peak is related to the amount of the specific nucleus in the region of interest.

Theoretically, all nuclei with nonzero spin can be employed for magnetic resonance imaging and spectroscopy, with adjustment of scanner hardware and sequences to select the nucleus-specific frequency and to enable imaging with sufficient signal-to-noise ratio. Hence, besides conventional proton resonance spectroscopy (^{1}H MRS) that represents a powerful technique to study myocardial content of metabolites, such as lipids and creatine in vivo [1, 13, 17, 18, 56, 125], MRS has also been successfully developed in rodent models of cardiovascular diseases for the study of various other nuclei, including ^{13}C, ^{19}F, ^{31}P and ^{23}Na. These nuclei are mostly investigated to noninvasively map regional metabolic processes in vivo, through combination with ^{1}H MRI acquisitions

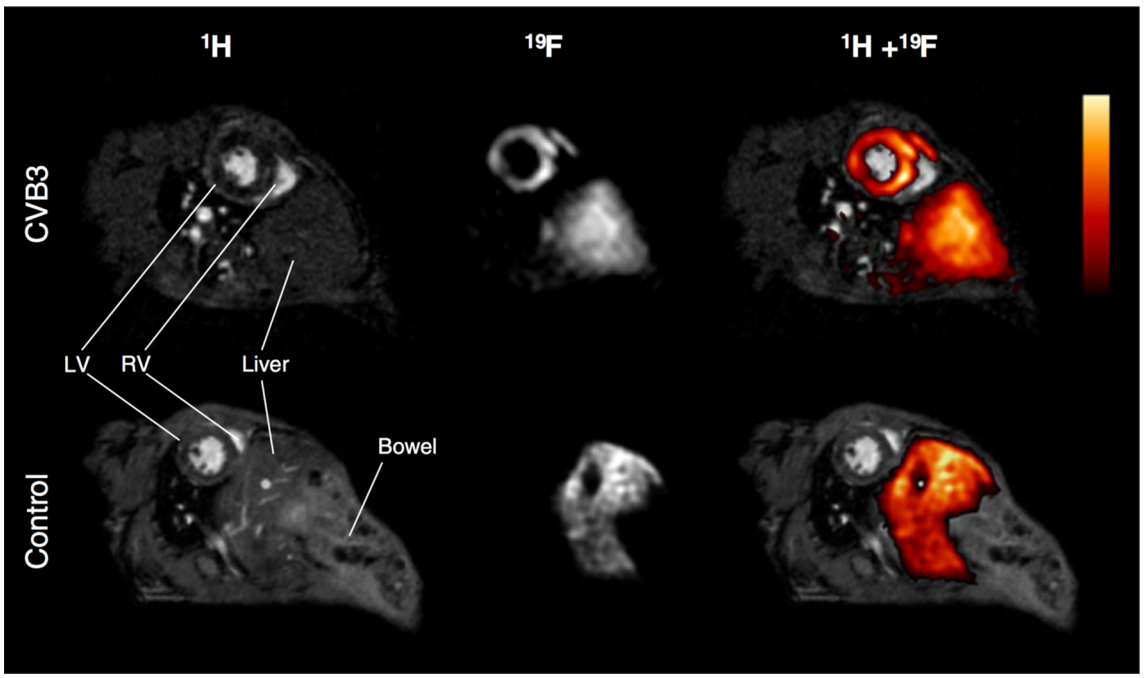

Fig. 6 Short-axis ^{1}H and ^{19}F MR images from a mouse thorax 14 days after inducing myocarditis by injection of coxsackievirus B3 and two days after application of PFCs (*top row*). Merged images (*right*) clearly show a homogenous accumulation of PFCs within the left ventricular wall of treated animals, whereas no ^{19}F signal was observed within the heart of control animals (*bottom*). Reproduced with permission from Jacoby et al. [70]

providing anatomic information. The combination of both techniques has brought the term of magnetic resonance spectroscopic imaging (MRSI).

^{13}C MRS of infused hyperpolarized 1-^{13}C-pyruvate, allows to monitor activity of the pyruvate dehydrogenase complex, as is reflects myocardial use of carbohydrates and their contribution to energetic homeostasis [16, 45]. Low intrinsic sensitivity of ^{13}C requires combined use of hyperpolarization techniques such as dynamic nuclear polarization (DNP) [10].

^{19}F MRI combined with injection of perfluorocarbon (PFC) allows study of inflammatory processes in the context of cardiac ischemia [50], myocarditis (Fig. 6) [70, 153], atherosclerotic [152] or thromboembolic processes [142]. PFCs are inert, nontoxic carbohydrates with fluorine that are phagocytized by circulating cells. As ^{19}F is virtually absent in tissue from animals and humans, fluorine can be detected without any background and with direct proportionality to the amount of ^{19}F nuclei present in the tissue, allowing quantitative measurement, whereas use

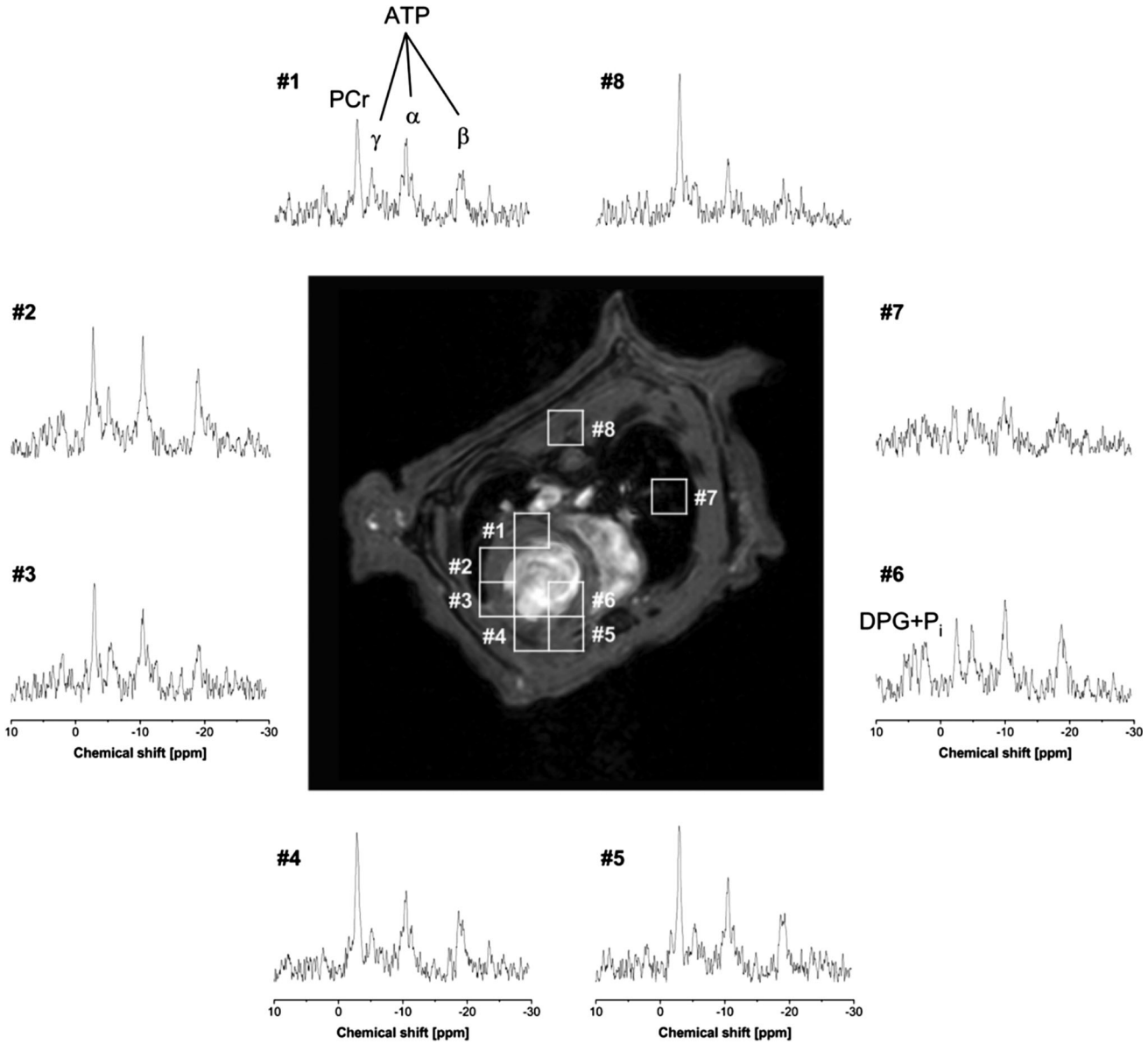

Fig. 7 Representative ^{31}P MR spectra from selected voxels of the mouse thorax superimposed with the anatomical ^{1}H MR image acquired in the same examination. Spatially localized spectra of the posterior (*#1*), lateral (*#2* and *#3*), and anterior (*#4* and *#5*) walls, and the septum (*#6*) of the heart are displayed. Additionally, spectra from the lungs (*#7*) and the skeletal muscle of the animal's back (*#8*) are shown. Reproduced with permission from Flögel et al. [51]

of gadolinium and oxide-based contrast agents relies on relaxation time alterations and nonlinear dose–signal response are often seen at high concentration. Furthermore, transition into clinical applications is likely feasible for ^{19}F MRSI, as PFC exhibit a high safety profile according to preliminary experiments, while concerns related to toxicity and safety could limit the use of other contrast agents to humans.

The analysis of ATP and phosphocreatine in tissue samples is problematic because of the instability of these molecules. Therefore, the principal method for measuring components of cardiac energy metabolism remains phosphorus-31 magnetic resonance spectroscopy ^{31}P MRS [108]. This well-established method has already been applied to various mouse models to study in vivo cardiac energetic metabolism, as assessed by the PCr/ATP ratio [1, 15, 16, 42, 51]. Representative ^{31}P MR spectra from selected regions of the mouse thorax superimposed with the anatomical ^{1}H MR image are shown in Fig. 7.

^{23}Na MRS reflects the activity of the sodium–potassium pump (Na^+/K^+-ATPase). As disruption of normal electrochemical gradients indicates cellular injury or dysfunction, following regional concentration of Na could provide precocious information regarding myocardial viability. Precise localization of infarction could be performed by observing the changes in the magnitude of sodium signal, since Na concentration is increased by >200 % in infarcted area [81]. Up to now, only technical studies have been reported on mice [94, 109], but recent methodological improvements suggest that further studies on models of myocardial infarction could soon be available.

Of note, MRS using other nuclei have been subject to preliminary development in small animals, inter alia oxygen-17 (^{17}O) [93] and rubidium-87 (^{87}Rb) MRS [78]. Detailed description of these techniques is beyond the scope of this review.

Chemical exchange saturation transfer (CEST) MRI

Besides spectroscopy, current development of chemical exchange saturation transfer (CEST) MRI techniques in cardiovascular research could allow multiplexed molecular imaging in a single session [158]. CEST-MRI takes advantage of the transfer of magnetization from endogenous macromolecules, chemical contrast agents or engineered reporter genes with nearby water molecules to generate contrast on MRI, with a higher sensitivity compared to MRS [91].

Perspectives: fast acquisitions and multimodal imaging

Improving imaging speed: parallel imaging, compressed sensing (CS) and cryoprobes

An important issue when considering MRI imaging of small animals is the need to simplify the manipulations, especially by shortening acquisition time of sequences. Various approaches have been studied for that purpose. Here, we describe those that are currently the most successful in mice.

Parallel imaging exploits the multiple elements of a phased array coil. Each element is associated with an independent radiofrequency pathway whose signals can be processed and combined together. A combination of such overlapping multiple receiver coil elements can be utilized to improve the signal-to-noise ratio and allows to speed up acquisitions as the number of spatial encoding steps can be decreased and conventional Fourier encoding reduced [40, 124].

Other techniques aim to specifically reduce the amount of acquired data without degrading the image quality. Indeed, compressed sensing (CS) allows to reconstruct images from significantly fewer measurements than were traditionally thought necessary, by exploiting the redundancy of the image in space or time. Signals and images are reconstructed with good accuracy from these measurements through a nonlinear procedure. The increasing and successful use of this method to improve cardiovascular MRI characterization of small animal models suggests that it will continue to expand in the near future.

Cryoprobe is a technology where the RF coil and/or preamplifier are cooled with a stream of Helium gas. As a consequence, the coil performance is improved and the level of thermal noise generated by the associated electronics is reduced. This allows significantly shorter measurement times and improvement of in vivo resolution compared to room temperature conventional probes. If its use may reduce the available space within the magnet, studies have shown that cardiovascular studies on small animals with a cryoprobe were feasible at HF [167].

Multimodal imaging

Now that several HF MRI sequences are routinely used for the characterization of murine models, their combination to get fundamental energetics, functional and anatomic cardiac information for the same animal promises to be an important in vivo tool for assessing the physiological relevance of structural and functional modifications and the

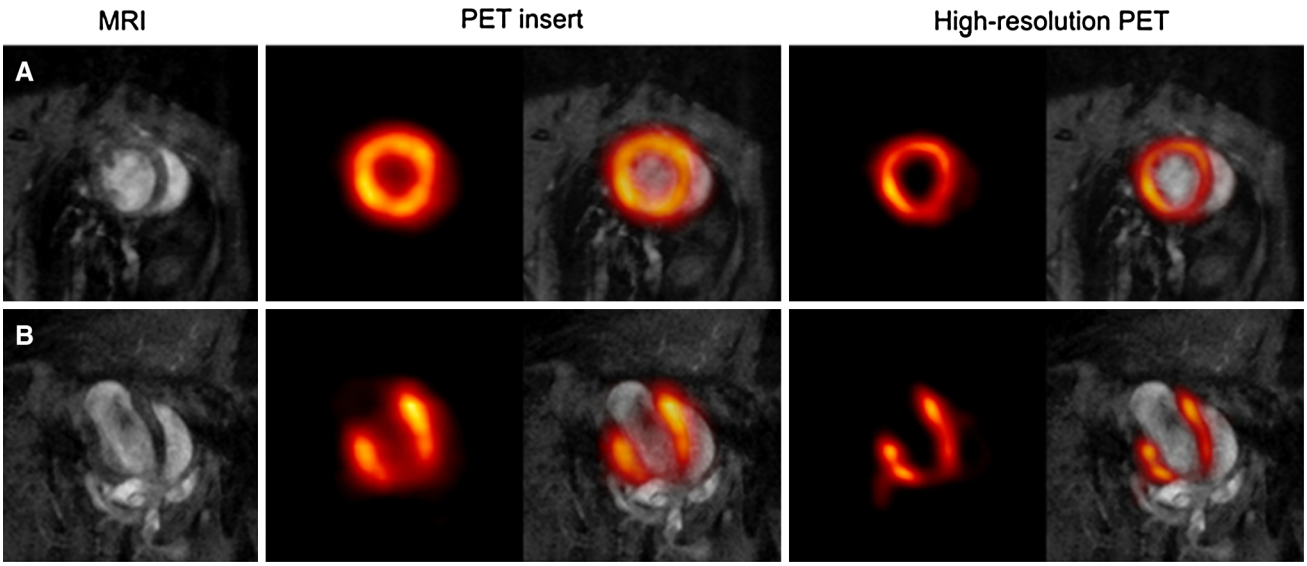

Fig. 8 Sample coregistered ^{18}F FDG PET and ^{1}H MR images at 7 T in a mouse model of myocardial infarction. **a** Short-axis view. **b** Long-axis view. Reproduced with permission from Büscher et al. [31]

usefulness of therapeutic interventions. Besides the classical coupling of ^{1}H-MRI with MRS of other nuclei to get spatially encoded metabolic information, several other studies combining different imaging modalities on the same animal models have recently exemplified the power multimodal imaging [25, 105, 160, 161].

Beyond the use of multimodality MRI examination, the combination of MRI with another imaging technology such as positron emission tomography (PET) results in a promising hybrid molecular imaging tool, taking advantage of both the high-resolution cardiovascular imaging of MRI and the high sensitivity of PET for sparse molecular or cellular targets. Compared to computed tomography (CT) imaging, classically combined with PET, MRI is more flexible due to its plurality of sequences and offers improved contrast [157, 171]. PET/MRI also enables dual target molecular imaging by simultaneous use of MRI agents [146]. While PET and MR imaging can be done sequentially with offline fusion of data, newer scanners allow for synchronous data acquisitions in mice (Fig. 8).

Integrating PET and MRI technologies is more complex than the evolution towards multimodality PET-CT due to the presence of the magnetic field, explaining the slow progress to efficient systems. Historically, the first approach for simultaneous PET/MR used optical fibers guiding the scintillation light to the photomultiplier tubes—important elements of standard PET detectors—outside the MRI [127]. Further improvements, mainly initiated by the advent of avalanche photodiodes allowed the operation of magnetic field insensitive PET detectors inside the MRI bore [172].

Sequential [95, 146] or combined use of PET and MRI [31, 97] has been reported to study various issues on the mouse models of cardiovascular diseases at HF. In light of this success, manufacturers will probably propose more automated tools for combined PET/MRI imaging in the near future.

Conclusions

We provided a comprehensive overview of HF MRI sequences available for cardiovascular investigation in mice, with practical information and reference literature for researchers wishing to implement this tool in their practice.

Despite the many challenges encountered when moving to higher field strength and small animal imaging, HF MRI has undoubtedly become an essential technique in cardiovascular research, as evidenced by the extensive literature on the subject in recent years. Because of the huge ongoing development in the field, further refinement of the technique will allow even wider opportunities in basic animal research.

Acknowledgments The authors thank Hassan Jassar and Nicolas Joudiou for assistance during MRI manipulations. This work was supported by Grants from the Fonds de la Recherche Scientifique FRS-FNRS, the Foundation Saint-Luc and the Belgian National Foundation for Research in Pediatric Cardiology.

Compliance with ethical standards

Conflict of interest No potential conflicts of interest were disclosed.

Animal studies All institutional and national guidelines for the care and use of laboratory animals were followed and approved by the appropriate institutional committees. No human studies were carried out by the authors for this article.

References

1. Abdurrachim D, Ciapaite J, Wessels B, Nabben M, Luiken JJ, Nicolay K, Prompers JJ (2014) Cardiac diastolic dysfunction in high-fat diet fed mice is associated with lipotoxicity without impairment of cardiac energetics in vivo. Biochim Biophys Acta 1842:1525–1537. doi:10.1016/j.bbalip.2014.07.016
2. Abeykoon S, Sargent M, Wansapura JP (2012) Quantitative myocardial perfusion in mice based on the signal intensity of flow sensitized CMR. J Cardiovasc Magn Reson 14:73. doi:10.1186/1532-429X-14-73
3. Aguor EN, Arslan F, van de Kolk CW, Nederhoff MG, Doevendans PA, van Echteld CJ, Pasterkamp G, Strijkers GJ (2012) Quantitative T2* assessment of acute and chronic myocardial ischemia/reperfusion injury in mice. MAGMA 25:369–379. doi:10.1007/s10334-012-0304-0
4. Akki A, Gupta A, Weiss RG (2013) Magnetic resonance imaging and spectroscopy of the murine cardiovascular system. Am J Physiol Heart Circ Physiol 304:H633–H648. doi:10.1152/ajpheart.00771.2011
5. Aletras AH, Ding S, Balaban RS, Wen H (1999) DENSE: displacement encoding with stimulated echoes in cardiac functional MRI. J Magn Reson 137:247–252. doi:10.1006/jmre.1998.1676
6. Alsaid H, Sabbah M, Bendahmane Z, Fokapu O, Felblinger J, Desbleds-Mansard C, Corot C, Briguet A, Cremillieux Y, Canet-Soulas E (2007) High-resolution contrast-enhanced MRI of atherosclerosis with digital cardiac and respiratory gating in mice. Magn Reson Med 58:1157–1163. doi:10.1002/mrm.21308
7. Amundsen BH, Ericsson M, Seland JG, Pavlin T, Ellingsen O, Brekken C (2011) A comparison of retrospectively self-gated magnetic resonance imaging and high-frequency echocardiography for characterization of left ventricular function in mice. Lab Anim 45:31–37. doi:10.1258/la.2010.010094
8. Andrews M, Giger ML, Roman BB (2015) Manganese-enhanced MRI detection of impaired calcium regulation in a mouse model of cardiac hypertrophy. NMR Biomed 28:255–263. doi:10.1002/nbm.3249
9. Antkowiak P, Janiczek R, Gibberman L, Xu C, Kramer C, Meyer C, French B, Epstein F (2010) Quantitative first-pass perfusion MRI of the mouse heart. J Cardiovasc Magn Reson 12:M10
10. Ardenkjaer-Larsen JH, Fridlund B, Gram A, Hansson G, Hansson L, Lerche MH, Servin R, Thaning M, Golman K (2003) Increase in signal-to-noise ratio of >10,000 times in liquid-state NMR. Proc Natl Acad Sci USA 100:10158–10163. doi:10.1073/pnas.1733835100
11. Axel L, Dougherty L (1989) MR imaging of motion with spatial modulation of magnetization. Radiology 171:841–845. doi:10.1148/radiology.171.3.2717762
12. Azam S, Desjardins CL, Schluchter M, Liner A, Stelzer JE, Yu X, Hoit BD (2012) Comparison of velocity vector imaging echocardiography with magnetic resonance imaging in mouse models of cardiomyopathy. Circ Cardiovasc Imaging 5:776–781. doi:10.1161/CIRCIMAGING.111.972406
13. Bakermans AJ, Abdurrachim D, Geraedts TR, Houten SM, Nicolay K, Prompers JJ (2015) In vivo proton T1 relaxation times of mouse myocardial metabolites at 9.4 T. Magn Reson Med 73:2069–2074. doi:10.1002/mrm.25340
14. Bakermans AJ, Abdurrachim D, Moonen RP, Motaal AG, Prompers JJ, Strijkers GJ, Vandoorne K, Nicolay K (2015) Small animal cardiovascular MR imaging and spectroscopy. Prog Nucl Magn Reson Spectrosc 88–89:1–47. doi:10.1016/j.pnmrs.2015.03.001
15. Bakermans AJ, Abdurrachim D, van Nierop BJ, Koeman A, van der Kroon I, Baartscheer A, Schumacher CA, Strijkers GJ, Houten SM, Zuurbier CJ, Nicolay K, Prompers JJ (2015) In vivo mouse myocardial P MRS using three-dimensional image-selected in vivo spectroscopy (3D ISIS): technical considerations and biochemical validations. NMR Biomed. doi:10.1002/nbm.3371
16. Bakermans AJ, Dodd MS, Nicolay K, Prompers JJ, Tyler DJ, Houten SM (2013) Myocardial energy shortage and unmet anaplerotic needs in the fasted long-chain acyl-CoA dehydrogenase knockout mouse. Cardiovasc Res 100:441–449. doi:10.1093/cvr/cvt212
17. Bakermans AJ, Geraedts TR, van Weeghel M, Denis S, Joao Ferraz M, Aerts JM, Aten J, Nicolay K, Houten SM, Prompers JJ (2011) Fasting-induced myocardial lipid accumulation in long-chain acyl-CoA dehydrogenase knockout mice is accompanied by impaired left ventricular function. Circ Cardiovasc Imaging 4:558–565. doi:10.1161/CIRCIMAGING.111.963751
18. Bakermans AJ, van Weeghel M, Denis S, Nicolay K, Prompers JJ, Houten SM (2013) Carnitine supplementation attenuates myocardial lipid accumulation in long-chain acyl-CoA dehydrogenase knockout mice. J Inherit Metab Dis 36:973–981. doi:10.1007/s10545-013-9604-4
19. Baltes C, Bosshard S, Mueggler T, Ratering D, Rudin M (2011) Increased blood oxygen level-dependent (BOLD) sensitivity in the mouse somatosensory cortex during electrical forepaw stimulation using a cryogenic radiofrequency probe. NMR Biomed 24:439–446. doi:10.1002/nbm.1613
20. Bauer WR, Hiller KH, Galuppo P, Neubauer S, Kopke J, Haase A, Waller C, Ertl G (2001) Fast high-resolution magnetic resonance imaging demonstrates fractality of myocardial perfusion in microscopic dimensions. Circ Res 88:340–346
21. Bauer WR, Roder F, Hiller KH, Han H, Frohlich S, Rommel E, Haase A, Ertl G (1997) The effect of perfusion on T1 after slice-selective spin inversion in the isolated cardioplegic rat heart: measurement of a lower bound of intracapillary-extravascular water proton exchange rate. Magn Reson Med 38:917–923
22. Beyers RJ, Smith RS, Xu Y, Piras BA, Salerno M, Berr SS, Meyer CH, Kramer CM, French BA, Epstein FH (2012) T(2)-weighted MRI of post-infarct myocardial edema in mice. Magn Reson Med 67:201–209. doi:10.1002/mrm.22975
23. Blain A, Greally E, Laval S, Blamire A, Straub V, MacGowan GA (2013) Beta-blockers, left and right ventricular function, and in vivo calcium influx in muscular dystrophy cardiomyopathy. PLoS One 8:e57260. doi:10.1371/journal.pone.0057260
24. Bohl S, Lygate CA, Barnes H, Medway D, Stork LA, Schulz-Menger J, Neubauer S, Schneider JE (2009) Advanced methods for quantification of infarct size in mice using three-dimensional high-field late gadolinium enhancement MRI. Am J Physiol Heart Circ Physiol 296:H1200–H1208. doi:10.1152/ajpheart.01294.2008
25. Bonner F, Jacoby C, Temme S, Borg N, Ding Z, Schrader J, Flogel U (2014) Multifunctional MR monitoring of the healing process after myocardial infarction. Basic Res Cardiol 109:430. doi:10.1007/s00395-014-0430-0
26. Bull E, Madani SY, Sheth R, Seifalian A, Green M, Seifalian AM (2014) Stem cell tracking using iron oxide nanoparticles. Int J Nanomedicine 9:1641–1653. doi:10.2147/IJN.S48979
27. Bulluck H, Maestrini V, Rosmini S, Abdel-Gadir A, Treibel TA, Castelletti S, Bucciarelli-Ducci C, Manisty C, Moon JC (2015) Myocardial T1 mapping. Circ J 79:487–494. doi:10.1253/circj.CJ-15-0054
28. Bun SS, Kober F, Jacquier A, Espinosa L, Kalifa J, Bonzi MF, Kopp F, Lalevee N, Zaffran S, Deharo JC, Cozzone PJ, Bernard M (2012) Value of in vivo T2 measurement for myocardial

fibrosis assessment in diabetic mice at 11.75 T. Invest Radiol 47:319–323. doi:10.1097/RLI.0b013e318243e062
29. Bunck AC, Engelen MA, Schnackenburg B, Furkert J, Bremer C, Heindel W, Stypmann J, Maintz D (2009) Feasibility of functional cardiac MR imaging in mice using a clinical 3 Tesla whole body scanner. Invest Radiol 44:749–756. doi:10.1097/RLI.0b013e3181b2c135
30. Buonincontri G, Hu C-H, Sawiak S, Krieg T (2014) P516Diastolic dysfunction in diabetic mice revealed by MRI. Cardiovasc Res 103 (Suppl 1):S94–S95
31. Buscher K, Judenhofer MS, Kuhlmann MT, Hermann S, Wehrl HF, Schafers KP, Schafers M, Pichler BJ, Stegger L (2010) Isochronous assessment of cardiac metabolism and function in mice using hybrid PET/MRI. J Nucl Med 51:1277–1284. doi:10.2967/jnumed.110.076448
32. Campbell-Washburn AE, Price AN, Wells JA, Thomas DL, Ordidge RJ, Lythgoe MF (2013) Cardiac arterial spin labeling using segmented ECG-gated look-locker FAIR: variability and repeatability in preclinical studies. Magn Reson Med 69:238–247. doi:10.1002/mrm.24243
33. Cassidy PJ, Schneider JE, Grieve SM, Lygate C, Neubauer S, Clarke K (2004) Assessment of motion gating strategies for mouse magnetic resonance at high magnetic fields. J Magn Reson Imaging 19:229–237. doi:10.1002/jmri.10454
34. Chacko VP, Aresta F, Chacko SM, Weiss RG (2000) MRI/MRS assessment of in vivo murine cardiac metabolism, morphology, and function at physiological heart rates. Am J Physiol Heart Circ Physiol 279:H2218–H2224
35. Chapon C, Herlihy AH, Bhakoo KK (2008) Assessment of myocardial infarction in mice by late gadolinium enhancement MR imaging using an inversion recovery pulse sequence at 9.4 T. J Cardiovasc Magn Reson 10:6. doi:10.1186/1532-429X-10-6
36. Chen J, Jia ZY, Ma ZL, Wang YY, Teng GJ (2011) In vivo serial MR imaging of magnetically labeled endothelial progenitor cells homing to the endothelium injured artery in mice. PLoS One 6:e20790. doi:10.1371/journal.pone.0020790
37. Chuang JS, Zemljic-Harpf A, Ross RS, Frank LR, McCulloch AD, Omens JH (2010) Determination of three-dimensional ventricular strain distributions in gene-targeted mice using tagged MRI. Magn Reson Med 64:1281–1288. doi:10.1002/mrm.22547
38. Cochet H, Montaudon M, Laurent F, Calmettes G, Franconi JM, Miraux S, Thiaudiere E, Parzy E (2010) In vivo MR angiography and velocity measurement in mice coronary arteries at 9.4 T: assessment of coronary flow velocity reserve. Radiology 254:441–448. doi:10.1148/radiol.2542090735
39. Coolen BF, Geelen T, Paulis LE, Nauerth A, Nicolay K, Strijkers GJ (2011) Three-dimensional T1 mapping of the mouse heart using variable flip angle steady-state MR imaging. NMR Biomed 24:154–162. doi:10.1002/nbm.1566
40. Coolen BF, Moonen RP, Paulis LE, Geelen T, Nicolay K, Strijkers GJ (2010) Mouse myocardial first-pass perfusion MR imaging. Magn Reson Med 64:1658–1663. doi:10.1002/mrm.22588
41. Coolen BF, Simonis FF, Geelen T, Moonen RP, Arslan F, Paulis LE, Nicolay K, Strijkers GJ (2014) Quantitative T2 mapping of the mouse heart by segmented MLEV phase-cycled T2 preparation. Magn Reson Med 72:409–417. doi:10.1002/mrm.24952
42. Cui W, Jang A, Zhang P, Thompson B, Townsend D, Metzger JM, Zhang J (2015) Early detection of myocardial bioenergetic deficits: a 9.4 Tesla complete non invasive 31P MR spectroscopy study in mice with muscular dystrophy. PLoS One 10:e0135000. doi:10.1371/journal.pone.0135000
43. Dall'Armellina E, Jung BA, Lygate CA, Neubauer S, Markl M, Schneider JE (2012) Improved method for quantification of regional cardiac function in mice using phase-contrast MRI. Magn Reson Med 67:541–551. doi:10.1002/mrm.23022
44. de Kemp RA, Epstein FH, Catana C, Tsui BM, Ritman EL (2010) Small-animal molecular imaging methods. J Nucl Med 51(Suppl 1):18S–32S. doi:10.2967/jnumed.109.068148
45. Dodd MS, Ball V, Bray R, Ashrafian H, Watkins H, Clarke K, Tyler DJ (2013) In vivo mouse cardiac hyperpolarized magnetic resonance spectroscopy. J Cardiovasc Magn Reson 15:19. doi:10.1186/1532-429X-15-19
46. Doty FD, Entzminger G, Kulkarni J, Pamarthy K, Staab JP (2007) Radio frequency coil technology for small-animal MRI. NMR Biomed 20:304–325. doi:10.1002/nbm.1149
47. Drelicharz L, Wozniak M, Skorka T, Tyrankiewicz U, Heinze-Paluchowska S, Jablonska M, Gebska A, Chlopicki S (2009) Application of magnetic resonance imaging in vivo for the assessment of the progression of systolic and diastolic dysfunction in a mouse model of dilated cardiomyopathy. Kardiol Pol 67:386–395
48. Epstein FH (2007) MR in mouse models of cardiac disease. NMR Biomed 20:238–255. doi:10.1002/nbm.1152
49. Ferreira VM, Piechnik SK, Robson MD, Neubauer S, Karamitsos TD (2014) Myocardial tissue characterization by magnetic resonance imaging: novel applications of T1 and T2 mapping. J Thorac Imaging 29:147–154. doi:10.1097/RTI.0000000000000077
50. Flogel U, Ding Z, Hardung H, Jander S, Reichmann G, Jacoby C, Schubert R, Schrader J (2008) In vivo monitoring of inflammation after cardiac and cerebral ischemia by fluorine magnetic resonance imaging. Circulation 118:140–148. doi:10.1161/CIRCULATIONAHA.107.737890
51. Flogel U, Jacoby C, Godecke A, Schrader J (2007) In vivo 2D mapping of impaired murine cardiac energetics in NO-induced heart failure. Magn Reson Med 57:50–58. doi:10.1002/mrm.21101
52. Gilliam AD, Epstein FH, Acton ST (2009) Cardiac motion recovery via active trajectory field models. IEEE Trans Inf Technol Biomed 13:226–235. doi:10.1109/TITB.2008.2009221
53. Gilson WD, Kraitchman DL (2007) Cardiac magnetic resonance imaging in small rodents using clinical 1.5 T and 3.0 T scanners. Methods 43:35–45. doi:10.1016/j.ymeth.2007.03.012
54. Gnyawali SC, Roy S, McCoy M, Biswas S, Sen CK (2009) Remodeling of the ischemia-reperfused murine heart: 11.7-T cardiac magnetic resonance imaging of contrast-enhanced infarct patches and transmurality. Antioxid Redox Signal 11:1829–1839. doi:10.1089/ARS.2009.2635
55. Gutjahr FT, Kampf T, Winter P, Meyer CB, Williams T, Jakob PM, Bauer WR, Ziener CH, Helluy X (2014) Quantification of perfusion in murine myocardium: a retrospectively triggered T-based ASL method using model-based reconstruction. Magn Reson Med. doi:10.1002/mrm.25526
56. Hankiewicz JH, Banke NH, Farjah M, Lewandowski ED (2010) Early impairment of transmural principal strains in the left ventricular wall after short-term, high-fat feeding of mice predisposed to cardiac steatosis. Circ Cardiovasc Imaging 3:710–717. doi:10.1161/CIRCIMAGING.110.959098
57. Hankiewicz JH, Goldspink PH, Buttrick PM, Lewandowski ED (2008) Principal strain changes precede ventricular wall thinning during transition to heart failure in a mouse model of dilated cardiomyopathy. Am J Physiol Heart Circ Physiol 294:H330–H336. doi:10.1152/ajpheart.01109.2007
58. Hankiewicz JH, Lewandowski ED (2007) Improved cardiac tagging resolution at ultra-high magnetic field elucidates transmural differences in principal strain in the mouse heart and reduced stretch in dilated cardiomyopathy. J Cardiovasc Magn Reson 9:883–890. doi:10.1080/10976640701693683
59. Heijman E, Aben JP, Penners C, Niessen P, Guillaume R, van Eys G, Nicolay K, Strijkers GJ (2008) Evaluation of manual and

automatic segmentation of the mouse heart from CINE MR images. J Magn Reson Imaging 27:86–93. doi:10.1002/jmri.21236
60. Herold V, Morchel P, Faber C, Rommel E, Haase A, Jakob PM (2006) In vivo quantitative three-dimensional motion mapping of the murine myocardium with PC-MRI at 17.6 T. Magn Reson Med 55:1058–1064. doi:10.1002/mrm.20866
61. Herold V, Parczyk M, Morchel P, Ziener CH, Klug G, Bauer WR, Rommel E, Jakob PM (2009) In vivo measurement of local aortic pulse-wave velocity in mice with MR microscopy at 17.6 Tesla. Magn Reson Med 61:1293–1299. doi:10.1002/mrm.21957
62. Herrmann KH, Schmidt S, Kretz A, Haenold R, Krumbein I, Metzler M, Gaser C, Witte OW, Reichenbach JR (2012) Possibilities and limitations for high resolution small animal MRI on a clinical whole-body 3 T scanner. MAGMA 25:233–244. doi:10.1007/s10334-011-0284-5
63. Hiba B, Richard N, Janier M, Croisille P (2006) Cardiac and respiratory double self-gated cine MRI in the mouse at 7 T. Magn Reson Med 55:506–513. doi:10.1002/mrm.20815
64. Hiba B, Richard N, Thibault H, Janier M (2007) Cardiac and respiratory self-gated cine MRI in the mouse: comparison between radial and rectilinear techniques at 7 T. Magn Reson Med 58:745–753. doi:10.1002/mrm.21355
65. Hoerr V, Nagelmann N, Nauerth A, Kuhlmann MT, Stypmann J, Faber C (2013) Cardiac-respiratory self-gated cine ultra-short echo time (UTE) cardiovascular magnetic resonance for assessment of functional cardiac parameters at high magnetic fields. J Cardiovasc Magn Reson 15:59. doi:10.1186/1532-429X-15-59
66. Howles GP, Ghaghada KB, Qi Y, Mukundan S Jr, Johnson GA (2009) High-resolution magnetic resonance angiography in the mouse using a nanoparticle blood-pool contrast agent. Magn Reson Med 62:1447–1456. doi:10.1002/mrm.22154
67. Hu TC, Bao W, Lenhard SC, Schaeffer TR, Yue TL, Willette RN, Jucker BM (2004) Simultaneous assessment of left-ventricular infarction size, function and tissue viability in a murine model of myocardial infarction by cardiac manganese-enhanced magnetic resonance imaging (MEMRI). NMR Biomed 17:620–626. doi:10.1002/nbm.933
68. Hu TC, Pautler RG, MacGowan GA, Koretsky AP (2001) Manganese-enhanced MRI of mouse heart during changes in inotropy. Magn Reson Med 46:884–890
69. Huby AC, Mendsaikhan U, Takagi K, Martherus R, Wansapura J, Gong N, Osinska H, James JF, Kramer K, Saito K, Robbins J, Khuchua Z, Towbin JA, Purevjav E (2014) Disturbance in Z-disk mechanosensitive proteins induced by a persistent mutant myopalladin causes familial restrictive cardiomyopathy. J Am Coll Cardiol 64:2765–2776. doi:10.1016/j.jacc.2014.09.071
70. Jacoby C, Borg N, Heusch P, Sauter M, Bonner F, Kandolf R, Klingel K, Schrader J, Flogel U (2014) Visualization of immune cell infiltration in experimental viral myocarditis by (19)F MRI in vivo. MAGMA 27:101–106. doi:10.1007/s10334-013-0391-6
71. Jacoby C, Boring YC, Beck A, Zernecke A, Aurich V, Weber C, Schrader J, Flogel U (2008) Dynamic changes in murine vessel geometry assessed by high-resolution magnetic resonance angiography: a 9.4 T study. J Magn Reson Imaging 28:637–645. doi:10.1002/jmri.21482
72. Jahnke C, Nagel E, Gebker R, Kokocinski T, Kelle S, Manka R, Fleck E, Paetsch I (2007) Prognostic value of cardiac magnetic resonance stress tests: adenosine stress perfusion and dobutamine stress wall motion imaging. Circulation 115:1769–1776. doi:10.1161/CIRCULATIONAHA.106.652016
73. Janiczek RL, Blackman BR, Roy RJ, Meyer CH, Acton ST, Epstein FH (2011) Three-dimensional phase contrast angiography of the mouse aortic arch using spiral MRI. Magn Reson Med 66:1382–1390. doi:10.1002/mrm.22937
74. Janssen BJ, De Celle T, Debets JJ, Brouns AE, Callahan MF, Smith TL (2004) Effects of anesthetics on systemic hemodynamics in mice. Am J Physiol Heart Circ Physiol 287:H1618–H1624. doi:10.1152/ajpheart.01192.2003
75. Janssen PM, Murray JD, Schill KE, Rastogi N, Schultz EJ, Tran T, Raman SV, Rafael-Fortney JA (2014) Prednisolone attenuates improvement of cardiac and skeletal contractile function and histopathology by lisinopril and spironolactone in the mdx mouse model of Duchenne muscular dystrophy. PLoS One 9:e88360. doi:10.1371/journal.pone.0088360
76. Jerosch-Herold M, Wilke N, Stillman AE (1998) Magnetic resonance quantification of the myocardial perfusion reserve with a Fermi function model for constrained deconvolution. Med Phys 25:73–84
77. Jiang K, Li W, Li W, Jiao S, Castel L, Van Wagoner DR, Yu X (2014) Rapid multislice T mapping of mouse myocardium: application to quantification of manganese uptake in alpha-Dystrobrevin knockout mice. Magn Reson Med. doi:10.1002/mrm.25533
78. Jilkina O, Xiang B, Kuzio B, Rendell J, Kupriyanov VV (2005) Potassium transport in Langendorff-perfused mouse hearts assessed by 87Rb NMR spectroscopy. Magn Reson Med 53:1172–1176. doi:10.1002/mrm.20450
79. Jung B, Odening KE, Dall'Armellina E, Foll D, Menza M, Markl M, Schneider JE (2012) A quantitative comparison of regional myocardial motion in mice, rabbits and humans using in vivo phase contrast CMR. J Cardiovasc Magn Reson 14:87. doi:10.1186/1532-429X-14-87
80. Kampf T, Helluy X, Gutjahr FT, Winter P, Meyer CB, Jakob PM, Bauer WR, Ziener CH (2014) Myocardial perfusion quantification using the T1 -based FAIR-ASL method: the influence of heart anatomy, cardiopulmonary blood flow and look-locker readout. Magn Reson Med 71:1784–1797. doi:10.1002/mrm.24843
81. Kim RJ, Lima JA, Chen EL, Reeder SB, Klocke FJ, Zerhouni EA, Judd RM (1997) Fast 23Na magnetic resonance imaging of acute reperfused myocardial infarction. Potential to assess myocardial viability. Circulation 95:1877–1885
82. Klink A, Heynens J, Herranz B, Lobatto ME, Arias T, Sanders HM, Strijkers GJ, Merkx M, Nicolay K, Fuster V, Tedgui A, Mallat Z, Mulder WJ, Fayad ZA (2011) In vivo characterization of a new abdominal aortic aneurysm mouse model with conventional and molecular magnetic resonance imaging. J Am Coll Cardiol 58:2522–2530. doi:10.1016/j.jacc.2011.09.017
83. Klink A, Hyafil F, Rudd J, Faries P, Fuster V, Mallat Z, Meilhac O, Mulder WJ, Michel JB, Ramirez F, Storm G, Thompson R, Turnbull IC, Egido J, Martin-Ventura JL, Zaragoza C, Letourneur D, Fayad ZA (2011) Diagnostic and therapeutic strategies for small abdominal aortic aneurysms. Nat Rev Cardiol 8:338–347. doi:10.1038/nrcardio.2011.1
84. Kohler S, Hiller KH, Griswold M, Bauer WR, Haase A, Jakob PM (2003) NMR-microscopy with TrueFISP at 11.75 T. J Magn Reson 161:252–257
85. Lairez O, Lonjaret L, Ruiz S, Marchal P, Franchitto N, Calise D, Fourcade O, Mialet-Perez J, Parini A, Minville V (2013) Anesthetic regimen for cardiac function evaluation by echocardiography in mice: comparison between ketamine, etomidate and isoflurane versus conscious state. Lab Anim 47:284–290. doi:10.1177/0023677213496236
86. Lefrancois W, Thiaudiere E, Ben Hassen W, Sanchez S, Franconi JM, Miraux S (2011) Fast whole-body magnetic resonance angiography in mice. Magn Reson Med 66:32–39. doi:10.1002/mrm.22985

87. Li W, Griswold M, Yu X (2012) Fast cardiac T1 mapping in mice using a model-based compressed sensing method. Magn Reson Med 68:1127–1134. doi:10.1002/mrm.23323
88. Li W, Griswold M, Yu X (2010) Rapid T1 mapping of mouse myocardium with saturation recovery look-locker method. Magn Reson Med 64:1296–1303. doi:10.1002/mrm.22544
89. Li W, Liu W, Zhong J, Yu X (2009) Early manifestation of alteration in cardiac function in dystrophin deficient mdx mouse using 3D CMR tagging. J Cardiovasc Magn Reson 11:40. doi:10.1186/1532-429X-11-40
90. Li W, Yu X (2010) Quantification of myocardial strain at early systole in mouse heart: restoration of undeformed tagging grid with single-point HARP. J Magn Reson Imaging 32:608–614. doi:10.1002/jmri.22256
91. Liu G, Song X, Chan KW, McMahon MT (2013) Nuts and bolts of chemical exchange saturation transfer MRI. NMR Biomed 26:810–828. doi:10.1002/nbm.2899
92. Look DC, Locker DR (1970) Time saving in measurement of NMR and EPR relaxation times. Rev Sci Instrum 41:250–251. doi:10.1063/1.1684482
93. Lu M, Atthe B, Mateescu GD, Flask CA, Yu X (2012) Assessing mitochondrial respiration in isolated hearts using (17)O MRS. NMR Biomed 25:883–889. doi:10.1002/nbm.1807
94. Maguire ML, Geethanath S, Lygate CA, Kodibagkar VD, Schneider JE (2015) Compressed sensing to accelerate magnetic resonance spectroscopic imaging: evaluation and application to 23Na-imaging of mouse hearts. J Cardiovasc Magn Reson 17:45. doi:10.1186/s12968-015-0149-6
95. Majmudar MD, Yoo J, Keliher EJ, Truelove JJ, Iwamoto Y, Sena B, Dutta P, Borodovsky A, Fitzgerald K, Di Carli MF, Libby P, Anderson DG, Swirski FK, Weissleder R, Nahrendorf M (2013) Polymeric nanoparticle PET/MR imaging allows macrophage detection in atherosclerotic plaques. Circ Res 112:755–761. doi:10.1161/CIRCRESAHA.111.300576
96. Mani V, Adler E, Briley-Saebo KC, Bystrup A, Fuster V, Keller G, Fayad ZA (2008) Serial in vivo positive contrast MRI of iron oxide-labeled embryonic stem cell-derived cardiac precursor cells in a mouse model of myocardial infarction. Magn Reson Med 60:73–81. doi:10.1002/mrm.21642
97. Maramraju SH, Smith SD, Junnarkar SS, Schulz D, Stoll S, Ravindranath B, Purschke ML, Rescia S, Southekal S, Pratte JF, Vaska P, Woody CL, Schlyer DJ (2011) Small animal simultaneous PET/MRI: initial experiences in a 9.4 T microMRI. Phys Med Biol 56:2459–2480. doi:10.1088/0031-9155/56/8/009
98. Messner NM, Zollner FG, Kalayciyan R, Schad LR (2014) Pre-clinical functional magnetic resonance imaging. Part II: the heart. Z Med Phys 24:307–322. doi:10.1016/j.zemedi.2014.06.008
99. Messroghli DR, Radjenovic A, Kozerke S, Higgins DM, Sivananthan MU, Ridgway JP (2004) Modified look-locker inversion recovery (MOLLI) for high-resolution T1 mapping of the heart. Magn Reson Med 52:141–146. doi:10.1002/mrm.20110
100. Moon JC, Messroghli DR, Kellman P, Piechnik SK, Robson MD, Ugander M, Gatehouse PD, Arai AE, Friedrich MG, Neubauer S, Schulz-Menger J, Schelbert EB, Society for Cardiovascular Magnetic Resonance I, Cardiovascular Magnetic Resonance Working Group of the European Society of C (2013) Myocardial T1 mapping and extracellular volume quantification: a Society for Cardiovascular Magnetic Resonance (SCMR) and CMR Working Group of the European Society of Cardiology consensus statement. J Cardiovasc Magn Reson 15:92. doi:10.1186/1532-429X-15-92
101. Moser E, Stahlberg F, Ladd ME, Trattnig S (2012) 7-T MR-from research to clinical applications? NMR Biomed 25:695–716. doi:10.1002/nbm.1794
102. Mosher TJ, Smith MB (1990) A DANTE tagging sequence for the evaluation of translational sample motion. Magn Reson Med 15:334–339
103. Motaal AG, Coolen BF, Abdurrachim D, Castro RM, Prompers JJ, Florack LM, Nicolay K, Strijkers GJ (2013) Accelerated high-frame-rate mouse heart cine-MRI using compressed sensing reconstruction. NMR Biomed 26:451–457. doi:10.1002/nbm.2883
104. Nahrendorf M, Hiller KH, Hu K, Ertl G, Haase A, Bauer WR (2003) Cardiac magnetic resonance imaging in small animal models of human heart failure. Med Image Anal 7:369–375
105. Nahrendorf M, Streif JU, Hiller KH, Hu K, Nordbeck P, Ritter O, Sosnovik D, Bauer L, Neubauer S, Jakob PM, Ertl G, Spindler M, Bauer WR (2006) Multimodal functional cardiac MRI in creatine kinase-deficient mice reveals subtle abnormalities in myocardial perfusion and mechanics. Am J Physiol Heart Circ Physiol 290:H2516–H2521. doi:10.1152/ajpheart.01038.2005
106. Naresh NK, Chen X, Roy RJ, Antkowiak PF, Annex BH, Epstein FH (2015) Accelerated dual-contrast first-pass perfusion MRI of the mouse heart: development and application to diet-induced obese mice. Magn Reson Med 73:1237–1245. doi:10.1002/mrm.25238
107. Naresh NK, Xu Y, Klibanov AL, Vandsburger MH, Meyer CH, Leor J, Kramer CM, French BA, Epstein FH (2012) Monocyte and/or macrophage infiltration of heart after myocardial infarction: MR imaging using T1-shortening liposomes. Radiology 264:428–435. doi:10.1148/radiol.12111863
108. Neubauer S (2007) The failing heart—an engine out of fuel. N Engl J Med 356:1140–1151. doi:10.1056/NEJMra063052
109. Neuberger T, Greiser A, Nahrendorf M, Jakob PM, Faber C, Webb AG (2004) 23Na microscopy of the mouse heart in vivo using density-weighted chemical shift imaging. MAGMA 17:196–200. doi:10.1007/s10334-004-0048-6
110. Nick H, Allegrini PR, Fozard L, Junker U, Rojkjaer L, Salie R, Niederkofler V, O'Reilly T (2009) Deferasirox reduces iron overload in a murine model of juvenile hemochromatosis. Exp Biol Med (Maywood) 234:492–503. doi:10.3181/0811-RM-337
111. Odintsov B, Chun JL, Mulligan JA, Berry SE (2011) 14.1 T whole body MRI for detection of mesoangioblast stem cells in a murine model of Duchenne muscular dystrophy. Magn Reson Med 66:1704–1714. doi:10.1002/mrm.22942
112. Ojha N, Roy S, Radtke J, Simonetti O, Gnyawali S, Zweier JL, Kuppusamy P, Sen CK (2008) Characterization of the structural and functional changes in the myocardium following focal ischemia-reperfusion injury. Am J Physiol Heart Circ Physiol 294:H2435–H2443. doi:10.1152/ajpheart.01190.2007
113. Okayama S, Nakano T, Uemura S, Fujimoto S, Somekawa S, Watanabe M, Nakajima T, Saito Y (2013) Evaluation of left ventricular diastolic function by fractional area change using cine cardiovascular magnetic resonance: a feasibility study. J Cardiovasc Magn Reson 15:87. doi:10.1186/1532-429X-15-87
114. Osman NF, Kerwin WS, McVeigh ER, Prince JL (1999) Cardiac motion tracking using CINE harmonic phase (HARP) magnetic resonance imaging. Magn Reson Med 42:1048–1060
115. Parzy E, Miraux S, Franconi JM, Thiaudiere E (2009) In vivo quantification of blood velocity in mouse carotid and pulmonary arteries by ECG-triggered 3D time-resolved magnetic resonance angiography. NMR Biomed 22:532–537. doi:10.1002/nbm.1365
116. Price AN, Cheung KK, Cleary JO, Campbell AE, Riegler J, Lythgoe MF (2010) Cardiovascular magnetic resonance imaging in experimental models. Open Cardiovasc Med J 4:278–292. doi:10.2174/1874192401004010278
117. Price AN, Cheung KK, Lim SY, Yellon DM, Hausenloy DJ, Lythgoe MF (2011) Rapid assessment of myocardial infarct size in rodents using multi-slice inversion recovery late gadolinium

enhancement CMR at 9.4 T. J Cardiovasc Magn Reson 13:44. doi:10.1186/1532-429X-13-44
118. Protti A, Sirker A, Shah AM, Botnar R (2010) Late gadolinium enhancement of acute myocardial infarction in mice at 7 T: cine-FLASH versus inversion recovery. J Magn Reson Imaging 32:878–886. doi:10.1002/jmri.22325
119. Rafael-Fortney JA, Chimanji NS, Schill KE, Martin CD, Murray JD, Ganguly R, Stangland JE, Tran T, Xu Y, Canan BD, Mays TA, Delfin DA, Janssen PM, Raman SV (2011) Early treatment with lisinopril and spironolactone preserves cardiac and skeletal muscle in Duchenne muscular dystrophy mice. Circulation 124:582–588. doi:10.1161/CIRCULATIONAHA.111.031716
120. Ruff J, Wiesmann F, Hiller KH, Voll S, von Kienlin M, Bauer WR, Rommel E, Neubauer S, Haase A (1998) Magnetic resonance microimaging for noninvasive quantification of myocardial function and mass in the mouse. Magn Reson Med 40:43–48
121. Salerno M, Kramer CM (2013) Advances in parametric mapping with CMR imaging. JACC Cardiovasc Imaging 6:806–822. doi:10.1016/j.jcmg.2013.05.005
122. Schmitter S, Wu X, Adriany G, Auerbach EJ, Ugurbil K, Moortele PF (2014) Cerebral TOF angiography at 7 T: impact of B1 (+) shimming with a 16-channel transceiver array. Magn Reson Med 71:966–977. doi:10.1002/mrm.24749
123. Schneider JE, Cassidy PJ, Lygate C, Tyler DJ, Wiesmann F, Grieve SM, Hulbert K, Clarke K, Neubauer S (2003) Fast, high-resolution in vivo cine magnetic resonance imaging in normal and failing mouse hearts on a vertical 11.7 T system. J Magn Reson Imaging 18:691–701. doi:10.1002/jmri.10411
124. Schneider JE, Lanz T, Barnes H, Stork LA, Bohl S, Lygate CA, Ordidge RJ, Neubauer S (2011) Accelerated cardiac magnetic resonance imaging in the mouse using an eight-channel array at 9.4 Tesla. Magn Reson Med 65:60–70. doi:10.1002/mrm.22605
125. Schneider JE, Tyler DJ, ten Hove M, Sang AE, Cassidy PJ, Fischer A, Wallis J, Sebag-Montefiore LM, Watkins H, Isbrandt D, Clarke K, Neubauer S (2004) In vivo cardiac 1H-MRS in the mouse. Magn Reson Med 52:1029–1035. doi:10.1002/mrm.20257
126. Shan K, Constantine G, Sivananthan M, Flamm SD (2004) Role of cardiac magnetic resonance imaging in the assessment of myocardial viability. Circulation 109:1328–1334. doi:10.1161/01.CIR.0000120294.67948.E3
127. Shao Y, Cherry SR, Farahani K, Meadors K, Siegel S, Silverman RW, Marsden PK (1997) Simultaneous PET and MR imaging. Phys Med Biol 42:1965–1970
128. Shea SM, Fieno DS, Schirf BE, Bi X, Huang J, Omary RA, Li D (2005) T2-prepared steady-state free precession blood oxygen level-dependent MR imaging of myocardial perfusion in a dog stenosis model. Radiology 236:503–509. doi:10.1148/radiol.2362040149
129. Skardal K, Rolim NP, Haraldseth O, Goa PE, Thuen M (2013) Late gadolinium enhancement in the assessment of the infarcted mouse heart: a longitudinal comparison with manganese-enhanced MRI. J Magn Reson Imaging 38:1388–1394. doi:10.1002/jmri.24127
130. Song R, Lin W, Chen Q, Asakura T, Wehrli FW, Song HK (2008) Relationships between MR transverse relaxation parameters R*(2), R(2) and R'(2) and hepatic iron content in thalassemic mice at 1.5 T and 3 T. NMR Biomed 21:574–580. doi:10.1002/nbm.1227
131. Song W, Dyer E, Stuckey D, Leung MC, Memo M, Mansfield C, Ferenczi M, Liu K, Redwood C, Nowak K, Harding S, Clarke K, Wells D, Marston S (2010) Investigation of a transgenic mouse model of familial dilated cardiomyopathy. J Mol Cell Cardiol 49:380–389. doi:10.1016/j.yjmcc.2010.05.009
132. Sosnovik DE, Dai G, Nahrendorf M, Rosen BR, Seethamraju R (2007) Cardiac MRI in mice at 9.4 Tesla with a transmit-receive surface coil and a cardiac-tailored intensity-correction algorithm. J Magn Reson Imaging 26:279–287. doi:10.1002/jmri.20966
133. Sosnovik DE, Nahrendorf M, Deliolanis N, Novikov M, Aikawa E, Josephson L, Rosenzweig A, Weissleder R, Ntziachristos V (2007) Fluorescence tomography and magnetic resonance imaging of myocardial macrophage infiltration in infarcted myocardium in vivo. Circulation 115:1384–1391. doi:10.1161/CIRCULATIONAHA.106.663351
134. Streif JU, Herold V, Szimtenings M, Lanz TE, Nahrendorf M, Wiesmann F, Rommel E, Haase A (2003) In vivo time-resolved quantitative motion mapping of the murine myocardium with phase contrast MRI. Magn Reson Med 49:315–321. doi:10.1002/mrm.10342
135. Streif JU, Nahrendorf M, Hiller KH, Waller C, Wiesmann F, Rommel E, Haase A, Bauer WR (2005) In vivo assessment of absolute perfusion and intracapillary blood volume in the murine myocardium by spin labeling magnetic resonance imaging. Magn Reson Med 53:584–592. doi:10.1002/mrm.20327
136. Stuckey DJ, Carr CA, Camelliti P, Tyler DJ, Davies KE, Clarke K (2012) In vivo MRI characterization of progressive cardiac dysfunction in the mdx mouse model of muscular dystrophy. PLoS One 7:e28569. doi:10.1371/journal.pone.0028569
137. Stuckey DJ, Carr CA, Tyler DJ, Clarke K (2008) Cine-MRI versus two-dimensional echocardiography to measure in vivo left ventricular function in rat heart. NMR Biomed 21:765–772. doi:10.1002/nbm.1268
138. Stuckey DJ, McSweeney SJ, Thin MZ, Habib J, Price AN, Fiedler LR, Gsell W, Prasad SK, Schneider MD (2014) T(1) mapping detects pharmacological retardation of diffuse cardiac fibrosis in mouse pressure-overload hypertrophy. Circ Cardiovasc Imaging 7:240–249. doi:10.1161/CIRCIMAGING.113.000993
139. Stypmann J (2007) Doppler ultrasound in mice. Echocardiography 24:97–112. doi:10.1111/j.1540-8175.2006.00358.x
140. Suever JD, Wehner GJ, Haggerty CM, Jing L, Hamlet SM, Binkley CM, Kramer SP, Mattingly AC, Powell DK, Bilchick KC, Epstein FH, Fornwalt BK (2014) Simplified post processing of cine DENSE cardiovascular magnetic resonance for quantification of cardiac mechanics. J Cardiovasc Magn Reson 16:94. doi:10.1186/s12968-014-0094-9
141. Tangney JR, Chuang JS, Janssen MS, Krishnamurthy A, Liao P, Hoshijima M, Wu X, Meininger GA, Muthuchamy M, Zemljic-Harpf A, Ross RS, Frank LR, McCulloch AD, Omens JH (2013) Novel role for vinculin in ventricular myocyte mechanics and dysfunction. Biophys J 104:1623–1633. doi:10.1016/j.bpj.2013.02.021
142. Temme S, Grapentin C, Quast C, Jacoby C, Grandoch M, Ding Z, Owenier C, Mayenfels F, Fischer JW, Schubert R, Schrader J, Flogel U (2015) Noninvasive imaging of early venous thrombosis by 19F magnetic resonance imaging with targeted perfluorocarbon nanoemulsions. Circulation 131:1405–1414. doi:10.1161/CIRCULATIONAHA.114.010962
143. ten Hove M, Lygate CA, Fischer A, Schneider JE, Sang AE, Hulbert K, Sebag-Montefiore L, Watkins H, Clarke K, Isbrandt D, Wallis J, Neubauer S (2005) Reduced inotropic reserve and increased susceptibility to cardiac ischemia/reperfusion injury in phosphocreatine-deficient guanidinoacetate-*N*-methyltransferase-knockout mice. Circulation 111:2477–2485. doi:10.1161/01.CIR.0000165147.99592.01
144. Troalen T, Capron T, Cozzone PJ, Bernard M, Kober F (2013) Cine-ASL: a steady-pulsed arterial spin labeling method for myocardial perfusion mapping in mice. Part I. Experimental study. Magn Reson Med 70:1389–1398. doi:10.1002/mrm.24565

145. Trotier AJ, Lefrancois W, Ribot EJ, Thiaudiere E, Franconi JM, Miraux S (2015) Time-resolved TOF MR angiography in mice using a prospective 3D radial double golden angle approach. Magn Reson Med 73:984–994. doi:10.1002/mrm.25201
146. Tucci S, Flogel U, Hermann S, Sturm M, Schafers M, Spiekerkoetter U (2014) Development and pathomechanisms of cardiomyopathy in very long-chain acyl-CoA dehydrogenase deficient (VLCAD(−/−)) mice. Biochim Biophys Acta 1842:677–685. doi:10.1016/j.bbadis.2014.02.001
147. Tyrankiewicz U, Skorka T, Jablonska M, Petkow-Dimitrow P, Chlopicki S (2013) Characterization of the cardiac response to a low and high dose of dobutamine in the mouse model of dilated cardiomyopathy by MRI in vivo. J Magn Reson Imaging 37:669–677. doi:10.1002/jmri.23854
148. Vallee JP, Ivancevic MK, Nguyen D, Morel DR, Jaconi M (2004) Current status of cardiac MRI in small animals. MAGMA 17:149–156. doi:10.1007/s10334-004-0066-4
149. van Bochove GS, Straathof R, Krams R, Nicolay K, Strijkers GJ (2010) MRI-determined carotid artery flow velocities and wall shear stress in a mouse model of vulnerable and stable atherosclerotic plaque. MAGMA 23:77–84. doi:10.1007/s10334-010-0200-4
150. van de Weijer T, van Ewijk PA, Zandbergen HR, Slenter JM, Kessels AG, Wildberger JE, Hesselink MK, Schrauwen P, Schrauwen-Hinderling VB, Kooi ME (2012) Geometrical models for cardiac MRI in rodents: comparison of quantification of left ventricular volumes and function by various geometrical models with a full-volume MRI data set in rodents. Am J Physiol Heart Circ Physiol 302:H709–H715. doi:10.1152/ajpheart.00710.2011
151. van Geuns RJ, Wielopolski PA, de Bruin HG, Rensing BJ, van Ooijen PM, Hulshoff M, Oudkerk M, de Feyter PJ (1999) Basic principles of magnetic resonance imaging. Prog Cardiovasc Dis 42:149–156
152. van Heeswijk RB, De Blois J, Kania G, Gonzales C, Blyszczuk P, Stuber M, Eriksson U, Schwitter J (2013) Selective in vivo visualization of immune-cell infiltration in a mouse model of autoimmune myocarditis by fluorine-19 cardiac magnetic resonance. Circ Cardiovasc Imaging 6:277–284. doi:10.1161/CIRCIMAGING.112.000125
153. van Heeswijk RB, Pellegrin M, Flogel U, Gonzales C, Aubert JF, Mazzolai L, Schwitter J, Stuber M (2015) Fluorine MR imaging of inflammation in atherosclerotic plaque in vivo. Radiology 275:421–429. doi:10.1148/radiol.14141371
154. van Nierop BJ, Coolen BF, Bax NA, Dijk WJ, van Deel ED, Duncker DJ, Nicolay K, Strijkers GJ (2014) Myocardial perfusion MRI shows impaired perfusion of the mouse hypertrophic left ventricle. Int J Cardiovasc Imaging 30:619–628. doi:10.1007/s10554-014-0369-0
155. van Nierop BJ, Coolen BF, Dijk WJ, Hendriks AD, de Graaf L, Nicolay K, Strijkers GJ (2013) Quantitative first-pass perfusion MRI of the mouse myocardium. Magn Reson Med 69:1735–1744. doi:10.1002/mrm.24424
156. van Oorschot JW, Gho JM, van Hout GP, Froeling M, Jansen Of Lorkeers SJ, Hoefer IE, Doevendans PA, Luijten PR, Chamuleau SA, Zwanenburg JJ (2015) Endogenous contrast MRI of cardiac fibrosis: beyond late gadolinium enhancement. J Magn Reson Imaging 41:1181–1189. doi:10.1002/jmri.24715
157. Vandenberghe S, Marsden PK (2015) PET-MRI: a review of challenges and solutions in the development of integrated multimodality imaging. Phys Med Biol 60:R115–R154. doi:10.1088/0031-9155/60/4/R115
158. Vandsburger M, Vandoorne K, Oren R, Leftin A, Mpofu S, Delli Castelli D, Aime S, Neeman M (2015) Cardio-chemical exchange saturation transfer magnetic resonance imaging reveals molecular signatures of endogenous fibrosis and exogenous contrast media. Circ Cardiovasc Imaging. doi:10.1161/CIRCIMAGING.114.002180
159. Vandsburger MH, Epstein FH (2011) Emerging MRI methods in translational cardiovascular research. J Cardiovasc Transl Res 4:477–492. doi:10.1007/s12265-011-9275-1
160. Vandsburger MH, French BA, Helm PA, Roy RJ, Kramer CM, Young AA, Epstein FH (2007) Multi-parameter in vivo cardiac magnetic resonance imaging demonstrates normal perfusion reserve despite severely attenuated beta-adrenergic functional response in neuronal nitric oxide synthase knockout mice. Eur Heart J 28:2792–2798. doi:10.1093/eurheartj/ehm241
161. Vandsburger MH, French BA, Kramer CM, Zhong X, Epstein FH (2012) Displacement-encoded and manganese-enhanced cardiac MRI reveal that nNOS, not eNOS, plays a dominant role in modulating contraction and calcium influx in the mammalian heart. Am J Physiol Heart Circ Physiol 302:H412–H419. doi:10.1152/ajpheart.00705.2011
162. Vandsburger MH, Janiczek RL, Xu Y, French BA, Meyer CH, Kramer CM, Epstein FH (2010) Improved arterial spin labeling after myocardial infarction in mice using cardiac and respiratory gated look-locker imaging with fuzzy C-means clustering. Magn Reson Med 63:648–657. doi:10.1002/mrm.22280
163. Vanhoutte L, Gallez B, Feron O, Balligand JL, Esfahani H, d'Hoore W, Moniotte S (2015) Variability of mouse left ventricular function assessment by 11.7 Tesla MRI. J Cardiovasc Transl Res. doi:10.1007/s12265-015-9638-0
164. Vlachopoulos C, Aznaouridis K, Stefanadis C (2010) Prediction of cardiovascular events and all-cause mortality with arterial stiffness: a systematic review and meta-analysis. J Am Coll Cardiol 55:1318–1327. doi:10.1016/j.jacc.2009.10.061
165. von Elverfeldt D, Maier A, Duerschmied D, Braig M, Witsch T, Wang X, Mauler M, Neudorfer I, Menza M, Idzko M, Zirlik A, Heidt T, Bronsert P, Bode C, Peter K, von Zur Muhlen C (2014) Dual-contrast molecular imaging allows noninvasive characterization of myocardial ischemia/reperfusion injury after coronary vessel occlusion in mice by magnetic resonance imaging. Circulation 130:676–687. doi:10.1161/CIRCULATIONAHA.113.008157
166. von Morze C, Xu D, Purcell DD, Hess CP, Mukherjee P, Saloner D, Kelley DA, Vigneron DB (2007) Intracranial time-of-flight MR angiography at 7 T with comparison to 3 T. J Magn Reson Imaging 26:900–904. doi:10.1002/jmri.21097
167. Wagenhaus B, Pohlmann A, Dieringer MA, Els A, Waiczies H, Waiczies S, Schulz-Menger J, Niendorf T (2012) Functional and morphological cardiac magnetic resonance imaging of mice using a cryogenic quadrature radiofrequency coil. PLoS One 7:e42383. doi:10.1371/journal.pone.0042383
168. Waghorn B, Edwards T, Yang Y, Chuang KH, Yanasak N, Hu TC (2008) Monitoring dynamic alterations in calcium homeostasis by T (1)-weighted and T (1)-mapping cardiac manganese-enhanced MRI in a murine myocardial infarction model. NMR Biomed 21:1102–1111. doi:10.1002/nbm.1287
169. Waghorn B, Yang Y, Baba A, Matsuda T, Schumacher A, Yanasak N, Hu TC (2009) Assessing manganese efflux using SEA0400 and cardiac T1-mapping manganese-enhanced MRI in a murine model. NMR Biomed 22:874–881. doi:10.1002/nbm.1414
170. Waller C, Kahler E, Hiller KH, Hu K, Nahrendorf M, Voll S, Haase A, Ertl G, Bauer WR (2000) Myocardial perfusion and intracapillary blood volume in rats at rest and with coronary dilatation: MR imaging in vivo with use of a spin-labeling technique. Radiology 215:189–197. doi:10.1148/radiology.215.1.r00ap07189
171. Wehrl HF, Judenhofer MS, Wiehr S, Pichler BJ (2009) Preclinical PET/MR: technological advances and new perspectives in biomedical research. Eur J Nucl Med Mol Imaging 36(Suppl 1):S56–S68. doi:10.1007/s00259-009-1078-0

172. Weissler B, Gebhardt P, Duppenbecker P, Wehner J, Schug D, Lerche C, Goldschmidt B, Salomon A, Verel I, Heijman E, Perkuhn M, Heberling D, Botnar R, Kiessling F, Schulz V (2015) A digital preclinical PET/MRI insert and initial results. IEEE Trans Med Imaging. doi:10.1109/TMI.2015.2427993
173. Wiesmann F, Neubauer S, Haase A, Hein L (2001) Can we use vertical bore magnetic resonance scanners for murine cardiovascular phenotype characterization? Influence of upright body position on left ventricular hemodynamics in mice. J Cardiovasc Magn Reson 3:311–315
174. Wiesmann F, Ruff J, Engelhardt S, Hein L, Dienesch C, Leupold A, Illinger R, Frydrychowicz A, Hiller KH, Rommel E, Haase A, Lohse MJ, Neubauer S (2001) Dobutamine-stress magnetic resonance microimaging in mice: acute changes of cardiac geometry and function in normal and failing murine hearts. Circ Res 88:563–569
175. Wiesmann F, Ruff J, Hiller KH, Rommel E, Haase A, Neubauer S (2000) Developmental changes of cardiac function and mass assessed with MRI in neonatal, juvenile, and adult mice. Am J Physiol Heart Circ Physiol 278:H652–H657
176. Zhao X, Pratt R, Wansapura J (2009) Quantification of aortic compliance in mice using radial phase contrast MRI. J Magn Reson Imaging 30:286–291. doi:10.1002/jmri.21846
177. Zhong J, Yu X (2010) Strain and torsion quantification in mouse hearts under dobutamine stimulation using 2D multiphase MR DENSE. Magn Reson Med 64:1315–1322. doi:10.1002/mrm.22530
178. Zhong X, Gibberman LB, Spottiswoode BS, Gilliam AD, Meyer CH, French BA, Epstein FH (2011) Comprehensive cardiovascular magnetic resonance of myocardial mechanics in mice using three-dimensional cine DENSE. J Cardiovasc Magn Reson 13:83. doi:10.1186/1532-429X-13-83